AD-A062 312 RENSSELAER POLYTECHNIC INST TROY N Y DEPT OF MATHEMA--ETC F/G 20/1
CONSISTENT ENVIRONMENTAL ACOUSTICS: APPLICATIONS TO STOCHASTIC --ETC(U)
DEC 78 W L SIEGMANN, M J JACOBSON, J G WATSON N00014-76-C-0288

UNCLASSIFIED RPI-MATH-121 NL

1 OF 1
ADA
062312

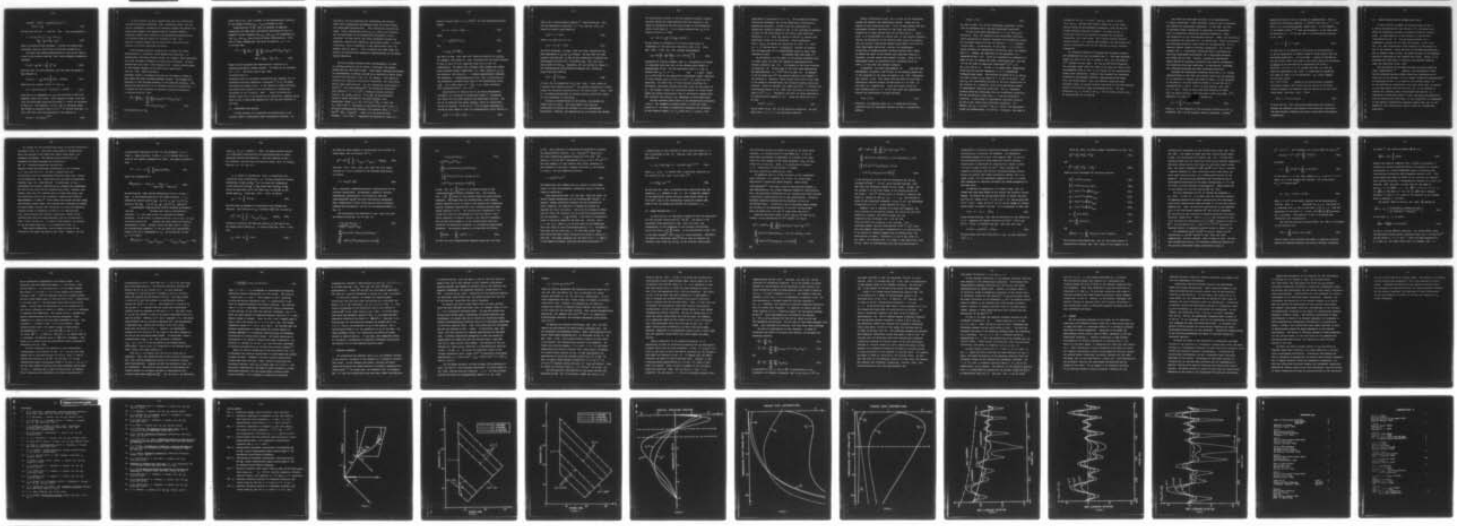

END
DATE
FILMED
3-79
DDC

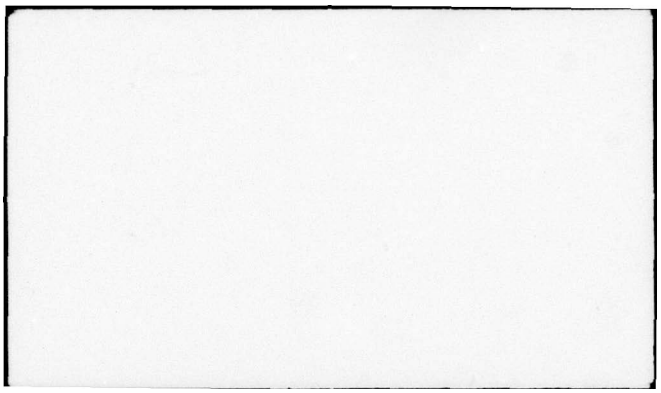

LEVEL II

20

(9) Technical rept.,

(6) Consistent Environmental Acoustics: Applications to Stochastic Internal-Wave Models.

by

(10) W. L./Siegmann, M. J./Jacobson
J. G./Watson

(11) 1 Dec 78

(12) 76p.

(14) RPI-MATH-121

Department of Mathematical Sciences
Rensselaer Polytechnic Institute
Troy, New York 12181

RPI Math. Rep. No. 121

December 1, 1978

This work was sponsored by
Code 222, Office of Naval Research
Contract No. (15) N 00014-76-C-0288
NR 386-606

408 898

ABSTRACT

A consistent environmental-acoustic model for a deep moving ocean is formulated. The acoustic model for regularly-perturbed SOFAR rays is approximately solved using a type of WKB(J) expansion. Interfacing conditions between the hydrodynamics and acoustics are developed which lead to constraints on acoustic frequency and transmission range. As an application, transmissions are considered through stochastic internal-wave fields, which have been modeled in a previously-published paper by the authors. Formulas for ray phase variances are derived. These formulas are asymptotically evaluated for rays with relatively significant depth variation, using the stationary phase method. New results are obtained for the dependence of the variances on internal-wave primitives, such as energy spectra. Expected multipath intensity is calculated for transmission through an ocean with static state modeled by a bilinear sound-speed profile. The effects of the internal-wave field and of varying internal-wave parameters on the expected intensity are shown to be significant.

INTRODUCTION

In recent years, oceanic environmental-acoustic models have been developed to consider a variety of phenomena, such as currents and internal waves. The objective of most of these studies is to predict variations in acoustical quantities, as for example intensity, when sound transmissions traverse an ocean region containing one or more environmental effects. The first principal purpose of this paper is to formulate a consistent environmental-acoustic model incorporating both sound-speed and velocity variations. Primary features of the model include its orientation toward deep-ocean transmissions, its foundation in ray acoustics, and its suitability for both deterministic and stochastic sound-speed and velocity fluctuations. A central and unique characteristic of the model is its emphasis on consistency. By a consistent analytic model, we mean one for which the model equations consistently include all terms and effects of a specified asymptotic order, and exclude all others of smaller order. Consistency must be observed in the environmental and acoustical portions of the model separately and in their relationship, or interfacing. As one example of the consequences of consistent interfacing, estimates can be found for the applicability of acoustic predictions, based on approximations made in determining expressions for sound-speed and velocity.

Our second principal objective is to apply our model to investigate features of sound transmission through a stochastic field of internal waves. Although much recent work has focused on this problem, many aspects have been incompletely resolved or overlooked entirely. For example, we know of only two acoustical treatments[1,2] which include velocity as well as sound-speed

fluctuations; the effects of the former, and the circumstances in which they are important, have not been sufficiently explored. A second example is our investigation of internal-wave effects on expected multipath intensity, which is evidently unique in the literature. As a third example, most analytic investigations[3-9] have used an internal-wave model first introduced in Ref. 10 and updated subsequently. The use of inconsistent approximations in that model, and acoustic work based on it, can be shown to significantly alter predictions for the acoustic quantities we investigate here. We note that our consistent approach differs from acoustic-fluctuation models that neglect explicit coupling to environmental effects (for example, as in portions of Refs. 11 and 12). Also, other acoustic internal-wave studies[13,14] have been directed toward parameter regions where ray theory may not be appropriate. At the beginning of Sec. III, we have listed six points, on at least one of which our development differs from each previous investigation.

In Sec. I, a ray acoustic model for moving media is formulated. Equations of the model are solved using a WKB(J)-type approximation under a number of explicitly stated assumptions. The application of the model to both deterministic and stochastic current and sound-speed fluctuations is discussed. Appropriate variable scales and model parameters are selected in Sec. II. Consistency and interfacing conditions on the acoustic and hydrodynamic parameters are discussed, and their constraints on CW source frequency and transmission range are illustrated. Useful simplifications based on consistency are presented. In Sec. III, we derive formulas for ray phase variances in the presence of a stochastic internal-wave field. Results are heavily based

on the consistent internal-wave model presented by the authors in a previous paper.[15] We define a class of rays with relatively significant depth variation, and asymptotically evaluate the phase variance for such rays in Sec. IV using the stationary phase method. From these results, we extract the specific internal-wave parameters which influence phase variance, discuss their effects, and compare our predictions to previous calculations. In Sec. V, we apply our phase variance results to the calculation of multipath expected intensity, assuming a bilinear static sound-speed profile. The effects of the internal-wave field and of varying internal-wave parameters on the range dependence of intensity are illustrated. Finally, our results are summarized in Sec. VI.

I. ACOUSTIC FORMULATION AND OCEAN APPLICATION

We consider the acoustic pressure $p(\vec{x},t)$, as a function of nondimensional position $\vec{x}$ and time t, in a medium with nondimensional sound speed $\bar{c}(\vec{x})$ and velocity, $\vec{u}(\vec{x})$ but with no attenuation or dispersion effects. Assuming the medium is unaffected by acoustic signal propagation, the nondimensional equation for p is [16]

$$\left\{\partial/\partial t + M(\vec{u}\cdot\nabla)\right\}^2 p = \bar{c}^{-2}\,\nabla^2 p\ , \tag{1}$$

where ∇ (∇^2) is the gradient operator (Laplacian). The dimensional position, sound speed, velocity, and time are nondimensionalized by the characteristic values X_0, c_0, U_0, and X_0/c_0, respectively, all to be specified later. The Mach number $M \equiv U_0/c_0$ is the ratio of the characteristic velocity to the characteristic sound speed and is assumed small. It is appropriate to expand the total sound speed $\bar{c}$ as a sum of a static term c_s and a velocity-induced term Mc, which we further expand in M:

$$\bar{c} = c_s + M[c^{(0)} + Mc^{(1)} + \ldots]\ . \tag{2a}$$

Similarly, the velocity $\vec{u}$ has the expansion

$$\vec{u} = \vec{u}^{(0)} + M\vec{u}^{(1)} + \ldots\ . \tag{2b}$$

The time dependence is separated from the spatial dependence in Eq. (1) by assuming p to be of the form

$$p(\vec{x},t) = \mathrm{Re}[\psi(\vec{x})\ \exp(-i\omega t)]\ , \tag{3a}$$

where Re denotes real part, i is the imaginary unit, and ω is

dimensionless angular frequency.

Substituting Eq. (3a) into Eq. (1), we obtain the reduced wave equation for ψ:

$$\bar{c}^2\nabla^2\psi + [\omega+iM(\vec{u}\cdot\nabla)]^2\psi = 0 \ . \tag{3b}$$

We restrict our attention to large values of ω, the geometric acoustics limit. We assume an asymptotic relation between M and ω^{-1}, $M = \omega^{-1}G(\omega^{-1})$, such that M is asymptotically order one with respect to ω^{-1}; i.e. as $\omega^{-1} \to 0$, $G \to F$ where F is a bounded constant. This assumption has been used for other acoustics problems, as in Ref. 17 for example. Substituting

into Eqs. (2) and (3b), the Mach number expansions of sound speed and velocity reduce to expansions in ω. To obtain an approximation for ψ, we use a type of WKB(J) expansion[18] in the parameter ω^{-1}. We assume that the complex function ψ has the polar form

$$\psi(\vec{x}) = \alpha(\vec{x}) \exp[i\phi(\vec{x})] \ , \tag{4a}$$

and expand the real functions amplitude $\alpha(\vec{x})$ and phase $\phi(\vec{x})$ as follows:

$$\alpha = \alpha^{(0)} + \omega^{-1}\alpha^{(1)} + \ldots \tag{4b}$$

and

$$\phi = \omega\tau + \phi^{(0)} + \omega^{-1}\phi^{(1)} + \ldots \ . \tag{4c}$$

The function $\omega\tau(\vec{x})$ is the principal contributor to the phase of ψ. The terms $\omega^{-j}\alpha^{(j)}$ and $\omega^{-j}\phi^{(j)}$ are order ω^{-j} corrections, and these

provide approximations to ψ and p correct to order ω^{-j}. Equations for τ, $\alpha^{(j)}$, and $\phi^{(j)}$ are obtained by substituting Eqs. (2) and (4) into Eq. (3b) and equating both real and imaginary parts of like powers of ω to zero.

We now focus on the order one solution for p, with brief consideration of higher order terms deferred to Sec. II. For convenience, variables c, $\vec{u}$, Φ, and α without superscripts hereafter represent those variables previously written with superscript zero. The equations obtained for τ, α, and Φ are

$$|\nabla\tau| = c_s^{-1} , \tag{5a}$$

$$\nabla\cdot(\alpha^2\nabla\tau) = 0 , \tag{5b}$$

and

$$\nabla\tau\cdot\nabla\Phi + F\, c_s^{-2}[\, c_s^{-1}c + \vec{u}\cdot\nabla\tau] = 0 \quad . \tag{5c}$$

The surfaces of constant phase are $\tau(\vec{x})$ = constant, and curves normal to these surfaces are the rays. Each ray describes a curve in space as a parameter, which we choose as arclength s, varies. Moreover, each ray is a member of a two-parameter family of curves, which we emphasize by denoting a ray as $\vec{x} = \vec{x}(s;\xi,\eta)$. The variables ξ and η parameterize the initial constant-phase surface, i.e. s = 0, from which all rays emanate. In this paper, we consider only rays that are continuously refracted, and mention later the modifications that arise if boundary reflections occur. In addition, we note the implicit assumption that the presence of the order M sound speed and currents produces a perturbation in a ray of regular, as opposed to singular, type. For example, we forbid the small fluctuations to change a ray from continuously

refracted to refracted/boundary-reflected type, or to cause a ray to disappear altogether.

Once the equation of a ray is known, the traditional form of the ray travel time $T(s;\xi,\eta) \equiv \tau[\vec{x}(s;\xi,\eta)]$ is obtained:

$$T = \int_0^s c_s^{-1} \, d\ell \ . \tag{6a}$$

In eq. (6a), the arguments of the integrand are ℓ, ξ, and η. Similarly, we obtain the order one phase along a ray, $\phi(s;\xi,\eta) \equiv \Phi[\vec{x}(s;\xi,\eta)]$:

$$\phi = - F \int_0^s \{c_s^{-2}(c + \vec{e}\cdot\vec{u})\} d\ell \ , \tag{6b}$$

where $\vec{e}(s;\xi,\eta) \equiv \partial\vec{x}(s;\xi,\eta)/\partial s$ is the unit tangent vector to a ray.

In order to find an expression for amplitude along a known ray, $A(s;\xi,\eta) = \alpha[\vec{x}(s;\xi,\eta)]$, we consider the important example of a point source. One model for a point source is a spherical initial phase surface of nondimensional radius $r = 1.0 \ m/X_0$. The pressure on this sphere is assumed a constant value which we choose as the scale for the nondimensional pressure, so that $A(0;\xi,\eta) = 1$. The parameters ξ and η are respectively taken as latitude and longitude on the sphere, so that $-\pi/2 \leq \xi \leq \pi/2$ and $0 \leq \eta \leq 2\pi$. For continuously-refracted rays emanating from a point source centered at $\vec{x} = \vec{x}_0$, the amplitude can be shown to be

$$A = r[c_s(\cos \xi)/c_0 \ J]^{1/2} \ . \tag{7a}$$

In Eq. (7a) $c_{\mathcal{J}} \equiv c_s(\vec{x}_{\mathcal{J}})$, and geometrical spreading loss is incorporated through J, the magnitude of the Jacobian of the ray parameterization,

$$J = \left| \frac{\partial \vec{x}}{\partial \xi} \times \frac{\partial \vec{x}}{\partial \eta} \cdot \vec{e} \right| \quad . \tag{7b}$$

The order one total acoustic pressure at a receiver located at $\vec{x} = \vec{x}_{\mathcal{R}}$ is constructed next, assuming a fixed CW point source at frequency ω. If $P(s,t;\xi,\eta) \equiv p[\vec{x}(s;\xi,\eta),t]$ is the order one acoustic pressure along a ray, then from Eqs. (3a) and (4)

$$P = A \cos\{\omega(T-t) + \phi\} \quad . \tag{8a}$$

The order one total pressure at the receiver, $\bar{p}(\vec{x}_{\mathcal{R}},t)$ is the sum of the contributions from individual rays. Let the set Λ be defined as

$$\Lambda = \{(s,\xi,\eta) \,|\, \vec{x}(s;\xi,\eta) = \vec{x}_{\mathcal{R}}\} \quad , \tag{8b}$$

and assume members of Λ can be labeled by integer values of an index n. If $P_{(n)}$ is the pressure corresponding to the n th member of Λ, then

$$\bar{p}(\vec{x}_{\mathcal{R}},t) = \sum_n P_{(n)} \quad . \tag{8c}$$

Other acoustic quantities of interest follow directly from Eqs. (8). For example, the total amplitude $\bar{\alpha}(\vec{x}_{\mathcal{R}})$ and total phase $\bar{\Phi}(\vec{\alpha}_{\mathcal{R}})$ at the receiver are related to $\bar{p}$ by Eqs. (3a) and (4a):

$$\bar{p}(\vec{x}_{\mathcal{R}},t) = \mathrm{Re}\{\bar{\alpha}(\vec{x}_{\mathcal{R}}) \exp[i(\bar{\Phi}(\vec{x}_{\mathcal{R}}) - \omega t)]\} \quad . \tag{9a}$$

Thus $\bar{\alpha}^2$, which is proportional to the acoustic intensity, is

$$\bar{\alpha}^2 = \left| \sum_n A_{(n)} \exp[i(\omega T_{(n)} + \phi_{(n)})] \right|^2 . \qquad (9b)$$

To specialize our moving-media acoustic formulation to deep-water oceanic transmission, we choose a Cartesian coordinate system with origin on the ocean surface. The positive x,y, and z axes are in the directions of east, north, and increasing depth, respectively, with unit vectors $\vec{i}$, $\vec{j}$, and $\vec{k}$ (Fig. 1). Also shown in Fig. 1 are the location of the source $\mathcal{S}$ at $\vec{x}_{\mathcal{S}} = (x_{\mathcal{S}}, y_{\mathcal{S}}, z_{\mathcal{S}})$ and the parameters ξ and η. The latter are spherical coordinates with zero values in the plane $z = z_{\mathcal{S}}$ and $y = y_{\mathcal{S}}$, respectively, and with increasing ξ values in the direction of increasing z.

The static sound speed in the ocean is well approximated by a function of depth only, $c_s = c_s(z)$. This simplification leads to the first integral of the ray equations, known as Snell's Law:

$$\cos\theta \,/\, \cos\xi = c_s(z) \,/\, c_{\mathcal{S}} , \qquad (10a)$$

where θ is the inclination angle of the ray, measured in the same sense as ξ (see Fig. 1). Since we consider only continuously refracted rays between fixed source and receiver, it can be shown that a unique value $\eta = \eta_s$ exists; i.e. rays are confined to the vertical plane containing source and receiver. We accentuate this symmetry by eliminating arclength as the ray parameter in favor of range R from the source, $R^2 \equiv (x - x_{\mathcal{S}})^2 + (y - y_{\mathcal{S}})^2$. If we regard $z = z(R;\xi)$ and $\theta = \theta(R;\xi)$ along a ray, it follows that

$$(dz/dR)^2 = \tan^2\theta = [c_{\mathcal{S}}(\sec\xi)/c_s(z)]^2 - 1,$$
$$z(0;\xi) = z_{\mathcal{S}} \quad . \tag{10b}$$

We note that the set Λ from Eq. (8b) may be expressed as

$$\Lambda = \{(\xi,\eta_s) \,|\, z(\chi,\xi) = z_{\mathcal{R}} \,,\, \tan\eta_s = (y_{\mathcal{R}} - y_{\mathcal{S}})/(x_{\mathcal{R}} - x_{\mathcal{S}})\} \quad , \tag{10c}$$

where the dimensionless parameter χ equals the dimensional horizontal range R_0 from source to receiver divided by X_0.

We obtain the leading approximation to the travel time of a ray to the receiver from Eq. (6a), after changing integration variable:

$$T(\chi,\xi) = c_{\mathcal{S}}\,(\sec\,\xi) \int_0^{\chi} c_s^{-2}\, dR \quad . \tag{11a}$$

From Eq. (6b), we find similarly that the order one phase at the receiver is

$$\phi(\chi;\xi,\eta) = -\, c_{\mathcal{S}}\, F\,(\sec\xi) \int_0^{\chi} c_s^{-3}(c + \vec{e}\cdot\vec{u})\,dR, \tag{11b}$$

where the unit tangent vector to a ray is

$$\vec{e} = (\cos\theta)[(\cos\eta_s)\vec{i} + (\sin\eta_s)\vec{j}] + (\sin\theta)\vec{k} \quad . \tag{11c}$$

Note that ϕ is independent of η_s if the functions c and $\vec{u}$ are symmetric about the z-axis. Both integrals in Eqs. (11a) and (11b) are evaluated using the ray paths $z = z(R;\xi)$ as solutions of Eqs.(10). The function J in Eq. (7b) is invariant under the change of parameter from s to R.[19] It follows from Eqs. (7), (10), and (11c) that the amplitude at the receiver is

$$A(\chi;\xi) = r\,|\chi(\partial z/\partial\xi)|^{-1/2} \quad . \tag{11d}$$

In this section, we have assumed that rays are continuously refracted and never reflected. When reflections occur, the ray can be considered a succession of segments between the reflections. Within each segment, our approach may be extended readily. Analogous formulas are found, but with appropriate modifications, one example being the limits of integrals in Eqs. (11). However, boundary models must be specified, along with their effects on acoustic amplitude and phase.

The foregoing acoustic formulation is useful for either deterministic or stochastic sound speeds and velocities. In applications involving internal waves, for example, these quantities are often regarded as members of statistical ensembles. We have assumed here only that c and $\vec{u}$ depend on $\vec{x}$. Precise specification of the ensemble depends on the particular application. From Eq. (11b), these stochastic processes induce a stochastic process for the phase ϕ, which in turn makes the total received pressure random. One example of a statistic of the received pressure is the expected intensity, with expectation defined here as an ensemble average and denoted by $\langle\ \rangle$. A formula for this quantity for general multipath propagation is obtained from Eq. (9b):

$$\langle \alpha^{-2} \rangle = \sum_n A_{(n)}^2 + \sum_{\substack{n \\ n \neq m}} \sum_m A_{(n)} A_{(m)} \cos\left[\omega(T_{(n)} - T_{(m)})\right] \cdot \langle \exp\left[i(\phi_{(n)} - \phi_{(m)})\right] \rangle \ . \qquad (12a)$$

The expectation on the

right side of Eq. (12a) is equal to the characteristic function of the random variable $\phi_{(n)} - \phi_{(m)}$ evaluated at one.

Simplification of Eq. (12a) is possible if specific assumptions are made about statistical properties of the ϕ's. Examples include assuming that $\phi_{(n)}$ and $\phi_{(m)}$ are independent or that $\phi_{(n)}$ and $\phi_{(m)}$ have bivariate normal distributions. With both of these assumptions, and using in addition $< \phi > = 0$, it follows that

$$< \bar{\alpha}^2 > = \sum_n A_{(n)}^2 + \sum_{\substack{n \\ n \neq m}} \sum_m A_{(n)} A_{(m)} \cos[\omega(T_{(n)} - T_{(m)})] \cdot \exp\left[-(\sigma_{(m)}^2 + \sigma_{(n)}^2)/2\right] , \qquad (12b)$$

where we have expressed the characteristic function of a normally-distributed random variable in terms of its variance, $\sigma^2 \equiv < \phi^2 >$. The first term in Eq. (12b) is proportional to intensity either if multipath interactions are ignored, i.e. if incoherent multipath summation is employed,[20] or if the phase variances are assumed large. In the absence of phase variances, the second term reduces to the contribution of interacting multipaths to the intensity. When phase variations are present, each term in the second sum is reduced by a damping factor which varies in magnitude depending on the ray pair involved in the term.

II. CONSISTENCY AND SCALING

In this section, we investigate the application of our acoustic model to deep-water ocean transmission problems. In

particular, we are concerned with interfacing the acoustic model and an appropriate hydrodynamic model for ocean current and sound-speed distributions. This interfacing involves two steps. First, appropriate scales X_0, U_0, and c_0 are selected, and the magnitudes of the dimensionless parameters ω and F estimated. We then verify that these parameters satisfy the asymptotic restrictions imposed by the acoustic model. A second interfacing step is necessary in many applications (see, for example, Refs.15 and 21). This is because the sound speed and current are obtained from asymptotic approximations of the hydrodynamic equations.

We first briefly consider ocean thermodynamics, in order to introduce notation and to obtain a consistent and general formulation for the static state. Sound speed, density, and pressure are thermodynamic variables related by an equation of state, which follows from relations in Ref. 22, for example. Such empirical equations are typically analytically cumbersome, but consistency permits some simplification. Let the dimensional sound speed c*, density ρ^*, and ocean pressure P^* be related by the generic state equation $c^* = c^*(\rho^*, P^*)$, assuming constant salinity. Further, let ρ_0, P_0, and $c_0 = c^*(\rho_0, P_0)$ be characteristic values of these variables at the ocean surface, with approximate values $\rho_0 = 1.02 \times 10^3$ kg m^{-3}, $P_0 = 1$ atm, and $c_0 = 1540$ m sec^{-1}. Analogous to the definition of $\bar{c}$ in Sec. I, we define nondimensional density $\bar{\rho}$ and pressure $\bar{P}$ by $\rho^* = \rho_0 \bar{\rho}$ and $P^* - P_0 = (\rho_0 g D) \bar{P}$, where g is the gravitational constant, 9.81 m sec^{-2}. Expanding the equation of state in a

Taylor's series about $\rho^* = \rho_0$ and $\rho^* = \rho_0$ and nondimensionalizing yields

$$\bar{c} = 1 + \nu(1-\bar{\rho}) + \Delta\mu\bar{\rho} + \ldots , \tag{13a}$$

where

$$\nu = - \rho_0 c_0^{-1} (\partial c^*/\partial \rho^*)_0 \tag{13b}$$

and

$$\mu = \rho_0 c_0 \, (\partial c^*/\partial \rho^*)_0 \quad . \tag{13c}$$

The zeros in Eqs. (13b) and (13c) denote evaluation at (ρ_0, ρ_0). For example, the values of ν and μ obtained from the state equation of Ref. 22 for a 35 o/oo isohaline ocean are 5.3 and 7.9, respectively. We remark that although these numbers may change with different oceanic conditions, i.e. other values of ρ_0, c_0, and salinity, the value of $\mu - \nu$ remains approximately constant. The parameter $\Delta = gD/c_0^2$ appearing in Eq. (13a) is the ratio of the hydrostatic pressure scale $\rho_0 gD$ to the thermodynamic scale $\rho_0 c_0^2$. For a deep ocean (D = 5 km), Δ is a small parameter, with approximate value 2.1×10^{-2}.

Specification of exactly one of the three thermodynamic variables, as a function of dimensional depth z^*, determines the others via the state equation and hydrostatic balance. One way is to prescribe the static density, which is conveniently written as follows. If we let $\hat{z} = z^*/D$ be depth nondimensionalized by total depth D, then the nondimensional static density is

$$\rho_s(\hat{z}) = 1 + \Delta(\hat{z} + \pi(\hat{z})) \quad , \tag{14a}$$

where $\pi(\hat{z})$ is the potential density.[21] Substituting Eq. (14a) and the hydrostatic result $\rho_s = \hat{z} + O(\Delta)$ into Eq. (13a), we obtain the static sound speed as

$$c_s(\hat{z}) = 1 + \Delta s(\hat{z}) \ , \tag{14b}$$

where s to order one in Δ is

$$s(z) = (\mu-\nu)\hat{z} - \nu\pi(\hat{z}) \ . \tag{14c}$$

The small parameter Δ in Eqs. (14a) and (14b) accentuates the weak dependence of ρ_s and c_s on depth. We note that for some acoustic applications, it may be more convenient to specify the sound-speed variation $s(\hat{z})$, from which Eqs. (14a) and (14c) may be used to find ρ_s. Equations (14) are written in terms of the nondimensional Brunt-Vaisala frequency $N(\hat{z})$ (scaled by g/c_0), using the identity

$$\pi(\hat{z}) = \int_0^{\hat{z}} N^2(s)ds \ . \tag{14d}$$

In fact, for an exponential N(z), Eqs. (14b) - (14d) reduce to a special case studied earlier.[23] Our general formulation is appropriate for arbitrary specification of the ocean static state. Also, it is readily generalized to include salinity variations, which are not considered in this paper.

Turning to specification of the scales, we consider the length scale X_0 first. The ocean depth D was used for convenience in scaling the variable $\hat{z}$ in the thermodynamic formulation. However, the appropriate X_0 is actually the minimum

of the plausible choices in the environmental-acoustic problem. The most obvious of these possibilities are, besides D, the range of transmission and the scale height of the dimensional static sound speed c_s^*. If we assume hereafter that R_0 is at least as large as D, then

$$X_0 = \text{Min}\ \{D,\ \max_{z^*} |c_s^*| / \max_{z^*} |dc_s^*/dz^*|\} \quad . \tag{15a}$$

We may obtain an estimate for the scale height which is independent of the particular functional form of c_s^*. Using Eqs. (14b) - (14d), Eq. (15a) becomes approximately

$$X_0 = \text{Min}\left\{D,\ c_0^2 g^{-1}\left[\max_{\hat{z}} |(\mu-\nu)-\nu N^2(\hat{z})|\right]^{-1}\right\} \quad . \tag{15b}$$

Estimating N^2 from, for example, Ref. 24, the quantity in braces is invariably less than ten, so the minimum scale height is approximately 25 km. For the deep-ocean value D = 5 km, it follows that $X_0 = D$, $z = \hat{z}$, and $\chi = R_0/D$. Since U_0 is prescribed by the appropriate hydrodynamic model, typically in value between 1.0cm sec^{-1} and 10 m sec^{-1}, all scales are now specified. We remark that if other physical processes are considered, additional possibilities may arise for the choice of X_0. For example, models for scattering effects of random sound-speed and current fluctuations lead to correlation lengths which may influence the choice of X_0, depending on their magnitudes.

We next consider restrictions on the dimensionless parameters ω and F. Our asymptotic acoustic model is valid for large values of ω. In terms of dimensional frequency and wavelength of the acoustic signal, $f_0 = c_0\,\omega/2\pi D$ and $\lambda_0 = c_0/2\pi f_0$, this

requirement is equivalent to $D >> \lambda_0$. This constraint forbids diffraction phenomena, one of the traditional limitations of geometrical acoustics. We note that the conditions for geometrical acoustics imposed in Ref. 25 are obtained by choosing X_0 equal to the scale height of the static sound speed and requiring $\omega >> 1$. Thus, our choice of smaller X_0 insures that conditions in Ref. 25 are satisfied. Having specified ω and $M = U_0/c_0$, we choose for simplicity $\omega M \equiv G(0) = F$. With $X_0 = D$, it follows that $F = 2\pi f_0 D U_0/c_0^2$. Further, we require that the magnitude of F is approximately unity or less, since otherwise M could be assumed other than order ω^{-1}.

We now define ε as the order of the maximum tolerable error we accept using our order one asymptotic approximation for acoustic pressure, Eqs. (8). An estimate of the error incurred in using Eqs. (8) is the order of the first term neglected by the approximation; i.e. $\omega^{-1} p^{(1)}(\vec{x},t)$ by Eqs. (4). In general, it can be shown that $p^{(1)}$ has secular behavior with respect to the variable $\vec{x}$. Moreover, these secular errors are of the order of the greatest nondimensional ray arclength between source and receiver. Since we consider only SOFAR rays here, it follows from calculations leading to Eq. (10b) that the order of the secular terms in $p^{(1)}$ is χ. Therefore, the order of terms neglected in our approximation reduces to $\chi\omega^{-1}$. Using the definition of ε, we have

$$O(\chi\omega^{-1}) \leq O(\varepsilon) , \qquad (16)$$

and we refer to Eq. (16) as the secularity condition. We note that since $\chi \geq 1$, $\omega >> 1$ as previously required.

Before illustration of Eq. (16), we turn to the consistency between the acoustic and hydrodynamic models. There are two aspects of this interfacing step. First, we must ensure that the hydrodynamic effects contribute to the order one acoustic pressure at an order greater than the acoustic error ε. Otherwise, it is inconsistent to include them in the acoustic analysis. Second, the derivation of the acoustic model implicitly assumes that the current $\vec{u}$ and motion-induced sound speed c are known as order Mach number quantities. However, the hydrodynamic derivations of models for these variables neglect small terms. We denote the order of the largest such neglected terms by γ. Therefore, we must insure that neglect of order γ terms in the hydrodynamic model is consistent with a tolerable error of order ε in the order one acoustic pressure.

To quantify the above requirements, we note that the hydrodynamic variables c and $\vec{u}$ occur in the acoustic model only in the integrand of the order one phase ϕ, Eq. (11b). Estimating the integral of Eq. (11b) shows that the order one and order γ hydrodynamic effects produce contributions to ϕ of order χF and order $\gamma\chi F$, respectively. Using this result in Eqs. (8) and expanding about $\chi F = 0$, we see that order one hydrodynamic effects are consistently included provided

$$O(\chi F) \geq O(\varepsilon). \qquad (17a)$$

Similarly, an expansion about $\gamma\chi F = 0$ yields the following inequality for the consistent neglect of order γ hydrodynamic effects:

$$O(\gamma\chi F) \leq O(\varepsilon) \ . \qquad (17b)$$

We refer to Eqs. (17) as the consistency conditions, noting that an expression for F has been determined previously.

For any given model application, g, D, c_0, and U_0 are specified. Thus, the secularity and consistency conditions place constraints on acoustic frequency and transmission range. We illustrate these first for the choices $\gamma = \varepsilon = \Delta$ (roughly one per cent). As motivation, we note that $\gamma = \Delta$ is often a useful estimate for hydrodynamic derivations (see, for example, Ref. 21). Indeed, the importance of the parameter Δ is suggested by Eqs. (14). Since our parameters are referred to a power of ten, we replace the order inequalities Eqs. (16) and (17) by the order of magnitude comparisons [26] $\chi\omega^{-1} \leq 3\Delta$, $\chi F \geq \Delta/3$, and $\chi F \leq 3$. In Fig. 2, we graph these inequalities, along with the earlier assumption $\chi \geq 1$, in dimensional frequency-range space. The previous estimates of g, D, and c_0 are used, as well as U_0 values of 1, 3, and 10 cm sec^{-1}. For each U_0, the simultaneous solution of the four inequalities is the interior of a trapezoid, which gives approximate ranges of experimental operating conditions. The U_0 - dependent parallel sides are determined from the consistency conditions, and the non-parallel sides from $\chi = 1$ and the secularity condition. A wide range of experimental operating values of R_0 and f_0 fall within each "interface trapezoid". For example, for $U_0 = 1$ cm sec^{-1} and $f_0 = 100$ Hz, the permissible ranges are approximately 5 to 650 km. Similarly, the range of

frequencies for U_0 = 3 cm sec^{-1} and R_0 = 200 km is about 30 to 560 Hz. We note that several values of U_0 are shown, because among the environmental parameters, this one has the largest possible relative variation. As shown in Fig. 2, decreasing values of U_0 typically increase the allowable frequencies, for fixed range. This results because smaller velocity scales, i.e. smaller Mach numbers, are associated with smaller fluctuations that can be resolved by higher acoustic frequencies.

To illustrate effects of changing the tolerable acoustic and hydrodynamic errors, we present Fig. 3. The same parameter values are used as in Fig. 2, except ε and γ are increased to $\Delta^{1/2}$ (roughly ten per cent). For any U_0 and fixed frequency, the allowable upper limit for range is at least as large as the corresponding value in Fig. 2, as a result of the significantly larger error tolerances. However, the boundary for consistent inclusion of hydrodynamic effects, represented by the lower line, has moved upward. Thus, the smaller range and lower frequency region is voided, because resolution of the environmental effects is diluted by larger permissible errors. For one comparison, U_0 = 1 cm sec^{-1} and f_0 = 100 Hz allows values of R_0 of approximately 30 to 1000 Km.

The cases just discussed are meant to be representative of typical conditions. Other parameter values or error tolerances may require new interfacing trapezoids. In any case, the role of systematic model interfacing is essential, as illustrated here in constraining acoustical operating conditions. Under the assumptions of our environmental-acoustic model, the constraints are necessary and sufficient for its application. Other investigators have developed different restrictions on the application of ray-theoretic models, based on different assumptions. For a recent example, Ref. 4 illustrates limitations due to scattering of rays from sound-speed fluctuations, for a particular internal-wave model and ray type. However, interfacing requirements supply additional necessary conditions that must be satisfied by the acoustical operating conditions. To the authors' knowledge, this interfacing process has been overlooked previously.

Provided the consistency conditions hold with $\gamma \geq \Delta$, further simplifications in the order one acoustic quantities are possible. It is consistent to neglect <u>all</u> terms of order γ in the integrand of the phase ϕ, not only those discarded in the derivations of expressions for c and $\vec{u}$. First, we note from Eq. (14b) that $c_s = 1 + O(\Delta)$. Since we have restricted attention to SOFAR rays, we obtain from Eq. (10a) that both ξ and θ are order $\Delta^{1/2}$. Therefore, to order γ, [illegible] reduces to:

$$\phi = - F \int_0^{\chi} (c + u_\eta + \theta w) dR \ , \qquad (18a)$$

where u_η is the component of the horizontal velocity in the η_s direction, and w is the vertical velocity component. Further,

suppose the oceanic flow is treated as incompressible. Then by scaling the continuity equation, it follows that $O(w/u_\eta) = \delta \equiv D/L$, where L is a horizontal dynamic length scale. If for example L is the Rossby radius,[15,21] then the parameter δ is the same order of magnitude as Δ. It follows that w is consistently neglected in Eq. (18a):

$$\phi = - F \int_0^\chi (c + u_\eta) dR \ . \tag{18b}$$

We note that in the process of evaluating or approximating ϕ, it may be appropriate to neglect terms of order greater than the previously-specified γ. In this event, γ should be replaced by the new larger value, and terms of this order should be eliminated <u>ab initio</u> in the derivations of expressions for $\vec{u}$ and c. Similarly, if also $\varepsilon \geq \Delta$, it follows from Eqs. (8) that the order one amplitude A, Eq. (11d), is simplified by neglecting all terms of order Δ in its evaluation. As a final example, we note that models for c and $\vec{u}$ often depend on the Brunt-Vaisala frequency. Consistency implies that values for the square of the Brunt-Vaisala frequency are obtained from the derivative of the static sound speed, using Eqs. (14b) - (14d):

$$N^2(z) = \nu^{-1}[(\mu-\nu)-s'(z)] \ . \tag{18c}$$

We note that Eq. (18c) explicitly demonstrates the connection between two essential environmental and acoustical quantities, the Brunt-Vaisala frequency and static sound-speed distribution, respectively.

III. PHASE VARIANCE FOR AN INTERNAL-WAVE FIELD

In this section, we apply the acoustic model of Sec. I to derive expressions for the variance σ^2 of the phase for a SOFAR ray propagating through a stochastic field of internal waves. An approximation to this quantity is derived and investigated in Sec. IV. The ray phase variance is of fundamental interest for at least two reasons. First, from Eqs. (11), the internal-wave field affects only the phase of a ray at the receiver. Since the mean of the phase perturbations due to internal waves is zero, the phase variance is the simplest statistic influenced by the internal wave field. Second, it is necessary and sufficient to determine the expected intensity under the conditions of Eq. (12b).

The calculation of ray phase variance has been treated by other investigators.[3-9] However, the development in this and the following section differs from their approaches in at least one of six features: (1) an "honest" stochastic approximation,[27] as formulated in Sec. I, is used for the acoustic model; (2) we are specifically interested in non-axial SOFAR rays, as opposed to just the special case of the axial ray; (3) we develop our results for a general static sound-speed distribution; (4) a consistent internal-wave model is used, including characteristics such as vertical mode structure; (5) our formulation is independent of the specific internal-wave spectral models used; and (6) the effects of the internal-wave velocity field are incorporated explicitly.

As a model for the internal-wave field, we use the formulation developed in Ref. 15. The static sound speed is deterministic, while the velocity $\vec{u}$ and order Mach number sound speed c are stochastic processes. The complete specifications of the ensembles for these processes are contained in Ref. 15. Principal properties include zero expected values and wide-sense stationarity in the variables x, y, and t but not in z. We wish to impose here the restrictions, such as continuously-refracting mean rays, regular ray perturbations, etc., under which the ray phase and amplitude formulas, Eqs. (11), were derived. In particular, in Sec. I sound-speed and current fluctuations are assumed time independent; but this is not valid for the internal-wave field. However, the dynamic time scale for internal waves is about four hours, and the correlation time of the stochastic internal-wave field is approximately 1.5 hours.[15] Since these time scales are much longer than acoustic travel times, the internal-wave field may be treated as quasi-steady, and any time variations in it may be studied by changing values of parameters by which it is characterized. Also, the horizontal and vertical correlation lengths of the internal-wave field are depth-dependent and are illustrated in Figs. 3 and 4 of Ref. 15. In view of those results, we continue to use the length scale $X_0 = D$, as specified in Sec. II.

Under above assumptions, the ray phase variance is the variance of the order one phase of Eq. (11b). However, for the

internal-wave formulation of Ref. 15, the parameter δ is of order Δ. Hence from Sec. II with $\gamma \geq \Delta$, it follows that ϕ is given by the simpler expression Eq. (18b). The phase variance is then

$$\sigma^2 = \langle \phi^2 \rangle = F^2 \int_0^X \int_0^X \mathcal{A}(R_1, R_2) dR_1 dR_2 , \qquad (19a)$$

where the integrand $\mathcal{A}$ is

$$\mathcal{A}(R_1, R_2; \xi) = \langle (c+u_\eta) \Big|_{(R_1, \xi, \eta_s)} (c+u_\eta) \Big|_{(R_2, \xi, \eta_s)} \rangle . \qquad (19b)$$

We note from Eq. (19b) and the definitions of R, ξ, η in Sec. I that $\mathcal{A}$ is the autocorrelation of the random function $c + u_\eta$ between the spatial points $[x_{\mathcal{A}} + R_1 \cos \eta_s, y_{\mathcal{A}} + R_1 \sin \eta_s, z_1(R_1, \xi)]$ and $[x_{\mathcal{A}} + R_2 \cos \eta_s, y_{\mathcal{A}} + R_2 \sin \eta_s, z_2(R_2, \xi)]$.

A considerable simplification of $\mathcal{A}$ is achieved by assuming that the internal wave field is horizontally isotropic, i.e. that there exists no preferred horizontal direction. In this case, it follows from Eq. (11) of Ref. 15 that the cross-correlation between the sound speed and velocity fluctuations is zero. Further, since the mean rays $z = z(R, \xi)$ are cylindrically symmetric, it can be shown with considerable algebra that $\mathcal{A}$ is independent of η_s. To evaluate $\mathcal{A}$, we set $\eta_s = 0$ to obtain

$$\mathcal{A}(R_1, R_2; \xi) = \langle c \Big|_{(R_1, \xi)} c \Big|_{(R_2, \xi)} \rangle + \langle u \Big|_{(R_1, \xi)} u \Big|_{(R_2, \xi)} \rangle , \qquad (19c)$$

where u_η at $\eta_s = 0$ equals u. Thus, the phase variance splits into individual contributions from autocorrelations of sound-speed and velocity fluctuations. This was observed in Ref. 1 for different internal-wave and acoustic models (see, for example, features (1), (4), and (5)).

It is useful to consider Eq. (19c) in connection with reciprocal sound transmissions, i.e. two-way propagation between hydrophones at $\vec{x}_S$ and $\vec{x}_R$.[2] Let the phase for propagation in the direction from $\vec{x}_S$ to $\vec{x}_R$ minus that from $\vec{x}_R$ to $\vec{x}_S$, along the same mean ray at the same time, be defined as the excess phase ϕ_E. Using Eqs. (11a) - (11c), we obtain

$$\phi_E = -2F \int_0^X \vec{e}\cdot\vec{u}\, dR , \qquad (20a)$$

and note that ϕ_E depends on fluctuations only through the velocity. The variance of ϕ_E is denoted by $\mathcal{E}^2$ and is given by

$$\mathcal{E}^2 = 4F^2 \int_0^X \int_0^X < u\big|_{(R_1,\xi)} u\big|_{(R_2,\xi)} > dR_1 dR_2 . \qquad (20b)$$

Similarly, we define the additive phase ϕ_A as the sum of the two phases used to define ϕ_E. It follows from Eqs. (11a) - (11c) that

$$\phi_A = 2\omega T - 2F \int_0^X c\, dR . \qquad (20c)$$

The additive phase depends on fluctuations only through the sound speed, and its variance a^2 is

$$a^2 = 4F^2 \int_0^X \int_0^X < c|_{(R_1,\xi)} \; c|_{(R_2,\xi)} > dR_1 dR_2 . \qquad (20d)$$

From Eqs. (19a), (19c), (20b), and (20d) the total phase variance of a ray is related to the variance constituents as follows:

$$\sigma^2 = 1/4(a^2 + \mathcal{E}^2) . \qquad (20e)$$

Thus, reciprocal transmissions permit interpretation of the variance constituents. Furthermore, suppose an acoustic experimental configuration is available so that the constituents a^2 and $\mathcal{E}^2$ are each individually measurable. Then, comparisons of their values may be used to estimate internal-wave parameters, as will be illustrated briefly in Sec. IV.

The autocorrelations appearing in Eqs. (20b) and (20d) are obtained from Eqs. (18) of Ref. 15:

$$< c(R_1,z_1)c(R_2,z_2) > = \qquad (21a)$$
$$2\nu^2 N_0^{-1} N^{3/2}(z_1) N^{3/2}(z_2) \cdot$$
$$\sum_{j=1}^{\infty} H(j/j^*) \sin[j\pi G(z_1)] \sin[j\pi G(z_2)] \cdot$$
$$\left\{ \int_1^{\infty} B(\hat{\omega})(1-\hat{\omega}^{-2}) J_0[\delta(R_2-R_1)\alpha(j,\hat{\omega})] d\hat{\omega} \right\}$$

and

$$< u(R_1,z_1)u(R_2,z_2) > = \tag{21b}$$

$$N_0^{-1}N^{1/2}(z_1)N^{1/2}(z_2) \cdot$$

$$\sum_{j=1}^{\infty} H(j/j^*)\cos[j\pi G(z_1)]\cos[j\pi G(z_2)] \cdot$$

$$\left\{ \int_1^{\infty} B(\hat{\omega}) \left[(1+\hat{\omega}^{-2}) J_0[\delta\ (R_2-R_1)\alpha(j,\hat{\omega})] \right.\right.$$

$$\left.\left. -(1-\hat{\omega}^{-2}) J_2[\delta\ (R_2-R_1)\alpha(j,\hat{\omega})] \right] d\hat{\omega} \right\} \quad .$$

In Eqs. (21), $N_0 = \int_0^1 N(z)dz$ is the depth average of the dimensionless Brunt-Vaisala frequency N(z). The function $G(z) \equiv N_0^{-1} \int_0^z N(s)ds$ is the average cumulative Brunt-Vaisala frequency. We assume that the internal-wave areal energy density spectrum $E(\hat{\omega},j)$ is equal to the product of a continuous marginal frequency spectrum $B(\hat{\omega})$ and a discrete marginal mode number spectrum $H(j/j^*)$. The internal-wave frequencies $\hat{\omega}$ are scaled such that one corresponds to twice the earth's local normal component of angular velocity (the inertial frequency). The vertical mode numbers j of the internal-wave field are scaled by the similarity parameter j*, an effective mode-number bandwidth. The marginal spectra are normalized as follows:

$$\int_1^{\infty} B(\hat{\omega})d\hat{\omega} = \sum_{j=1}^{\infty} H(j/j^*) = 1 \quad , \tag{21c}$$

so that the total dimensionless expected energy per unit area

is one. This condition is dimensionally satisfied by choosing the characteristic velocity $U_0 = (E_0/\rho_0 D)^{1/2}$, where E_0 is the total dimensional expected energy per unit area. The value $U_0 = 2.72$ cm sec^{-1} corresponds to $E_0 = 3.82 \times 10^3$ Jm^{-2}.[10] The wave numbers α of the internal wave field, appearing in the arguments of the order n Bessel functions J_n, are related to $\hat{\omega}$ and j via the dispersion relation

$$\alpha = j\pi N_0^{-1}(\hat{\omega}^2-1)^{1/2} \quad . \tag{21d}$$

The dimensional wave numbers are α/L, where L is the Rossby radius, so that the parameter δ multiplies $(R_2-R_1)\alpha$ after the range is scaled by D.

Upon substituting Eqs. (21) into Eqs. (20b) and (20d), we obtain lengthy expressions for the variances $\mathcal{A}^2$ and $\mathcal{E}^2$. In general, simpler analytical formulas are not available for these integrals, and numerical or asymptotic methods are employed for their evaluation. There are two classes of SOFAR rays for which the integrals can be analytically approximated. Let the parameter $\kappa \equiv \chi \underset{R}{\text{Max}} |dz/dR|$, the ratio of transmission range to the scale length of the mean ray. From Eq. (10b), $\kappa = \chi \tan |\theta_a|$, where θ_a is the ray angle at the SOFAR axis. The first class of rays is distinguished by $\kappa << 1$. Included in this case are the axial ray ($\kappa = 0$) and "near axial" rays with relatively small depth variation with range or values of χ near one. The range integrals for the axial ray z = a, where a is the SOFAR axis depth, have been evaluated previously.[6,7]

A second class of rays consists of those rays for which $\kappa \geq 1$, and is discussed in Sec. IV. From Eq. (10a) this condition is equivalent to

$$\chi \geq [c_a (\cos\xi)/c_{\mathcal{J}}] \cdot \{1 - [c_a(\cos\xi)/c_{\mathcal{J}}]^2\}^{-1/2} \qquad (22a)$$

where $c_a = c_s(a)$. It follows that a sufficient condition for the validity of Eq. (22a) is, to order $\Delta^{1/2}$,

$$\chi \geq [2(c_{\mathcal{J}} - c_a)]^{-1/2} . \qquad (22b)$$

We note that Eq. (22b) is typically more restrictive than the condition $\chi \geq 1$ assumed in Sec. II. For a numerical example, if the dimensional source and axial sound speeds differ by 30 m sec^{-1}, and if the transmission ranges are greater than about 25 km, all SOFAR rays satisfy the condition $\kappa \geq 1$.

IV. PHASE VARIANCE FOR $\kappa \geq 1$

In this section, we approximate asymptotically the expressions for the variance constituents $\mathcal{A}^2$ and $\mathcal{E}^2$. The phase of the sinusoidal terms appearing in Eqs. (21a) and (21b), and consequently in the integrands of the variance constituents, are of the form $j\pi N_0^{-1} \int_0^z N(s)ds$. In the derivations of Eqs. (21), it has been assumed[15] that $j\pi/N_0$ is a large parameter. Therefore, the method of stationary phase[28] may be used to simplify the integrals over range (R_1 and R_2) of the variance constituents.

The stationary points are values of R_1 and R_2 for which dz/dR vanishes, i.e. turning points of the SOFAR ray. It can be shown that this method is applicable if $\chi(dz/dR)$ is at least order one, with respect to the large parameter $j\pi/N_0$, at some values of R on the ray. Thus, it is sufficient to require $\kappa \geq 1$. Henceforth in this section, we assume the more restrictive condition Eq. (22b).

We emphasize that it is the inclusion of the j-dependent modal structure, c.f. feature (4) in Sec. III, which makes application of stationary phase feasible. Other recent investigations[4,5] have used a type of turning point method, an apex approximation, but without apparent asymptotic justification. Thus, the consistent formulation of our internal-wave model provides a theoretical justification for an apex approximation. Moreover, different numerical predictions are obtained, as will be illustrated later. In addition, use of stationary phase extends the validity of the approximation to include turning points below the SOFAR axis, not just to those above the axis.[4]

Applying stationary phase to first the R_1 and then the R_2 integral in the expressions for $\mathcal{A}^2$ and $\mathcal{E}^2$, we obtain

$$\mathcal{A}^2 = (8\nu^2F^2/\Delta) \sum_{\ell=1}^{K} \sum_{m=1}^{K} \Big[N(z_\ell)N(z_m)|S'(z_\ell)S'(z_m)|^{-1/2} \cdot$$

$$\sum_{j=1}^{\infty} [H(j/j^*)/j] \sin[j\pi G(z_\ell) \pm \pi/4] \sin[j\pi G(z_m) \pm \pi/4] \cdot$$

$$\Big\{ \int_1^{\infty} B(\hat{\omega})(1-\hat{\omega}^{-2}) J_0[\delta(R_m - R_\ell)\, \alpha(j,\hat{\omega})] d\hat{\omega} \Big\} \Big] \qquad (23a)$$

and

$$\mathcal{E}^2 = (4F^2/\Delta) \sum_{\ell=1}^{K} \sum_{m=1}^{K} \Bigg[|S'(z_\ell)S'(z_m)|^{-1/2} \cdot$$

$$\sum_{j=1}^{\infty} [H(j/j^*)/j] \cos[j\pi G(z_\ell) \pm \pi/4] \cos[j\pi G(z_m) \pm \pi/4] \cdot$$

$$\Bigg(\int_1^{\infty} B(\hat{\omega}) \Big\{ (1+\hat{\omega}^{-2}) J_0[\delta(R_m - R_\ell)\ \alpha(j,\hat{\omega})]$$

$$- (1-\hat{\omega}^{-2}) J_2[\delta(R_m - R_\ell)\alpha(j,\hat{\omega})] \Big\} d\hat{\omega} \Bigg) \Bigg] \quad . \qquad (23b)$$

In the derivation we have used the expression for the ray curvature $d^2z/dR^2 = -\Delta s'(z)$, which follows from Eqs. (10b) and (14b) and consistent neglect of $O(\Delta)$ terms. In Eqs. (23), the integer K is the total number of ray turning points for the range χ. The i^{th} turning point is located at range R_i and depth z_i, labeled so that $R_1 < R_2 < \cdots < R_K$. The choices of signs in the sinusoidal arguments, $j\pi G(z_i) \pm \pi/4$, are determined as positive if $s'(z_i) < 0$ and negative if $s'(z_i) > 0$.

Suppose a ray is regarded as divided into segments; the first consists of the portion between the source and the first SOFAR-axis crossing, the second between the next consecutive axis crossings, etc., and the last from the final axis crossing to the receiver. From stationary phase, the main contribution to $\mathcal{A}^2$ (or $\mathcal{E}^2$) from each ray segment comes from a neighborhood of its turning point. If an initial or terminal segment has no turning point, its contribution is absent. Therefore, in view of Eq. (20d) (or Eq. (20b)), we interpret the $\ell \neq m$ terms in the sums of Eq. (23a) (or Eq. (23b)) as contributions from the autocorrelations of

sound-speed (or velocity) fluctuations between neighborhoods of turning points in distinct ray segments. For physically interesting models of B and H (for example, Refs. 10 and 29), the autocorrelations of sound speed and velocity decrease significantly in magnitude for separations in depth of about 2 km and in range of about 15 km.[15] Thus, provided the respective horizontal and vertical distances between turning points are greater than these correlation lengths, the $\ell \neq m$ terms in Eqs. (23) are negligible compared to the $\ell = m$ terms. This assumption is typically satisfied for SOFAR propagation in the deep ocean.

In addition to neglecting $\ell \neq m$ terms in Eqs. (23), we assume that each mean SOFAR ray has exactly two distinct turning depths. We denote the turning depth above (or below) the axis by z^+ (or z^-), where $s'(z^+) < 0$ (or $s'(z^-) > 0$), and we note that $s(z^+) = s(z^-)$. Also, we let K^+ (or K^-) be the number of turning points above (or below) the axis. It is convenient to note that

$$s'(a) = 0 = (\mu-\nu) - \nu N^2(a) \quad , \tag{24a}$$

which follows from Eq. (18c) and the definition of the SOFAR axis $z = a$. Assuming the typical situation of $N^2(z^+) > N^2(a)$ and $N^2(z^-) < N^2(a)$, it follows from Eqs. (18c) and (24a) that

$$|s'(z^{\pm})| = \pm\nu[N^2(z^{\pm}) - N^2(a)] \ . \tag{24b}$$

We also define the ratio $N^2(z)/N^2(a) \equiv \beta(z)$, so that typically $\beta(z^{\pm}) \gtrless 1$.

Using Eq. (24b), we obtain compact expressions for Eqs. (23),

$$\mathcal{a}^2 = \mathcal{a}_0^2 \, [K^+ Q_c^+ + K^- Q_c^-] \tag{25a}$$

and

$$\mathcal{E}^2 = \mathcal{E}_0^2 \, [K^+ Q_u^+ + K^- Q_u^-] \, , \tag{25b}$$

where we have introduced the following notation:

$$\mathcal{a}_0^2 = 4\nu F^2 (1-I)/(\Delta J_*) \, , \tag{26a}$$

$$\mathcal{E}_0^2 = 2F^2 (1+I)/[(\mu-\nu)\Delta J_*] \, , \tag{26b}$$

$$Q_c^+ = \beta(\beta-1)^{-1}(1 + \mathcal{J}[G])\Big|_{z=z^+} \, , \tag{27a}$$

$$Q_c^- = \beta(1-\beta)^{-1}(1 - \mathcal{J}[G])\Big|_{z=z^-} \, , \tag{27b}$$

$$Q_u^+ = (\beta-1)^{-1}(1 - \mathcal{J}[G])\Big|_{z=z^+} \, , \tag{27c}$$

$$Q_u^- = (1-\beta)^{-1}(1 + \mathcal{J}[G])\Big|_{z=z^-} \, , \tag{27d}$$

$$I = \int_1^\infty [B(\hat{\omega})/\hat{\omega}^2] d\hat{\omega} \, , \tag{28a}$$

$$J_*^{-1} = \sum_{j=1}^{\infty} H(j/j^*)/j \, , \tag{28b}$$

and

$$\mathcal{J}[G(z)] = J_* \sum_{j=1}^{\infty} [H(j/j_*)/j] \sin [2\pi j G(z)] . \tag{28c}$$

The variance constituents Eqs. (25) are each proportional to normalization factors, Eqs. (26), which in turn depend on two

characteristic parameters of the internal-wave field, Eqs. (28a) and (28b). The number of upper and lower turning points appear in Eqs. (25) multiplied by Q factors, Eqs. (27). We note that typically SOFAR rays for relatively large source-receiver separations have more turning points than those for relatively small ranges. Thus, the linear dependence of $\mathcal{A}^2$ and $\mathcal{E}^2$ on K^+ and K^- reflects a general tendency for their increasing values with range, but their exact variation with χ is a complicated function of ray geometry. The quantity Q_c^+ represents the contribution due to sound-speed fluctuations at one upper turning point $z = z^+$, and the other Q's have analogous interpretations. These quantities in turn depend on β and the function $\mathcal{S}$, Eq. (28c).

The only dependence on $B(\hat{\omega})$ is through the parameter I, Eq. (28a). In Ref. 15, it is shown that the fractional amounts of expected potential and kinetic energies per unit horizontal area of the internal-wave field are equal to (1-I)/2 and (1+I)/2, respectively. Thus, the relative contributions of the spectrum $B(\hat{\omega})$ to the sound-speed dependent $\mathcal{A}^2$ and velocity dependent $\mathcal{E}^2$ are given by the fractions of expected potential and kinetic energies, respectively. Since $0 \leq I \leq 1$, the influence of $B(\hat{\omega})$ is to increase the contribution to σ^2 of $\mathcal{E}^2$, relative to that of $\mathcal{A}^2$. For the choice $B(\hat{\omega}) = 2(\pi\hat{\omega})^{-1}(\hat{\omega}^2-1)^{-1/2}$,[10] the ratio of expected kinetic to expected potential energy is three to one.

The dependence of $\mathcal{A}^2$ and $\mathcal{E}^2$ on $H(j/j_*)$ enters via the combinations J_* and $\mathcal{S}$, defined in Eqs. (28b) and (28c), respectively. We next consider each of these in turn. We note that interpreting $H(j/j_*)$ as a discrete probability density for the vertical mode-number energy distribution leads to

$J_*^{-1} = \langle 1/j \rangle$.[5] As an example, for Cairns' model of $H(j/j_*)$,[29]

$$H(j/j_*) = (j^2 + j_*^2)^{-1} / \sum_{j=1}^{\infty} (j^2+j_*^2)^{-1} , \tag{29a}$$

we obtain

$$J_* = \sum_{j=1}^{\infty} [j^2+j_*^2]^{-1} / \sum_{j=1}^{\infty} [j(j^2+j_*^2)]^{-1} . \tag{29b}$$

In the limit $j_* \to 0$, Eq. (29b) reduces to $J_* = \zeta(2)/\zeta(3) \simeq 1.37$, where $\zeta(n)$ is the Riemann zeta function. For large values of j_*, it follows that[30]

$$J_* \sim (\pi j_* - 1)/(2\gamma + \ln j_*^2) , \tag{29c}$$

where $\gamma = 0.557$ is the Euler constant, and the approximation from Eq. (29c) is excellent for $j_* \geq 4$. The value of J_* increases with j_*, and is less than j_* for $j_* \gtrsim 2$. From the appearance of the factor J_* in Eqs. (26), a_0^2 and $\mathcal{E}_0^2$ decrease as j_* increases. This behavior is due to increased mode interaction and "cancellation".

The vertical-structure function $\mathcal{A}(G)$, Eq. (28c), is analogous to the function $S(G)$,

$$S(G) = \sum_{j=1}^{\infty} H(j/j_*) \cos [2j\pi G] , \tag{30a}$$

which arises in the internal wave model to apportion relative amounts of expected potential and kinetic energies throughout

the depth.[15] The relation between $\mathcal{A}$ and S is

$$\mathcal{A}(G) = 2\pi J_* \int_0^G S(g)dg \ . \qquad (30b)$$

Whereas the spectral component $B(\hat{\omega})$, through the parameter I, reflects the relative expected energy contributions to variance constituents in a depth-independent manner, H modifies those contributions through the depth-dependent behavior of $\mathcal{A}$. This result explicitly shows an effect of our inclusion of internal-wave vertical structure, a consequence of feature (4) of Sec. III. From Eqs. (28b) and (28c), we note that for any model of $H(j/j_*) > 0$: (a) $|\mathcal{A}(G)| \leq 1$; (b) $\mathcal{A}(G) = 0$ for G = 0, 1/2, 1; (c) $\mathcal{A}(G)$ is odd about G = 1/2; and (d) $\mathcal{A}(G)$ has a maximum between G = 0 and G = 1/2, equal to the negative of its minimum, which is between G = 1/2 and 1.

For Cairns' model of $H(j/j_*)$, Eq. (29a), $\mathcal{A}$ reduces to

$$\mathcal{A}(G) = \pi J_* \left[\frac{(1-2G)\sinh(j_*\pi) - \sinh[j_*\pi(1-2G)]}{j_*\pi \cosh(j_*\pi) - \sinh(j_*\pi)} \right] \ . \qquad (31a)$$

In the limit $j_* \to 0$, we obtain

$$\mathcal{A}(G) = \frac{2\pi\zeta(2)}{\zeta(3)} [(1-2G)(G-G^2)] \ . \qquad (31b)$$

In Fig. 4, we plot $\mathcal{A}[G(z)]$ from Eqs. (31) versus depth, using the exponential Brunt-Vaisala frequency model $N(z) = 3/2 \exp(-4z)$[15] and the values $j_* = 0$, 3, and 7. Three has been suggested for j_* in Ref. 29, but other values (see, for example, Ref. 5)

may be appropriate, depending on the oceanic region. For reference, both the SOFAR axis depth, a = .26 from Eq. (24a), and the depth b = .17 for which G(b) = 1/2 are shown dashed. The values $\mu = 11.6$ and $\nu = 9.1$ in this example are obtained from Eqs. (14b) - (14d) by requiring that N(z) produce surface and axis sound speeds equal to 1540 and 1490 m sec^{-1}, respectively, in an ocean with D = 5 km and equal bottom and surface sound speeds. We note that the amplitude 3/2 of the exponential of N(z) has no influence on either b or $\mathcal{A}[G(z)]$, but it is necessary to determine the SOFAR axis. The curves in Fig. 4 possess the general characteristics of the previous paragraph. Their asymmetry in z results from the depth dependence of G(z). The situation a > b shown in Fig. 4 is in fact typical. Thus, typically there exist two types of upper turning points, corresponding to $0 < z^+ \leq b$ for which $\mathcal{A} \geq 0$, and $b < z^+ < a$, for which $\mathcal{A} < 0$. In addition, from Fig. 4 , we observe that as j_* increases, the maximum value of $|\mathcal{A}[G(z)]|$ decreases. This result is in concert with the cancellation effect discussed in connection with Eq. (29b).

We next investigate the behavior of the turning-point contributions, the Q factors of Eqs. (27). We note that they depend only on the specification of $H(j/j_*)$, N(z), a, and $z^{\pm}$, through the functions β and $\mathcal{A}$. We plot Eqs. (27) versus dimensionless upper turning-point depth z^+ in Fig. 5 , for $j_* = 3$ and the same example functions and other parameter values used in Fig. 4. Functions Q_c^+ (or Q_u^+) are shown solid (or dashed). The Q^- functions are evaluated at the lower turning-point z^-

corresponding to any z^+ (such that $s(z^-) = s(z^+)$) for the given mean sound-speed profile. The vertical-structure function $\mathcal{J}$ affects the Q's at all values of z^+. Its most important influence is on Q_c^+ and Q_u^- for z^+ between 0 and 0.1, at which depths $\mathcal{J}$ enhances Q_c^+ and detracts from Q_u^+. The sharp change in value of Q_c^+ near the surface is a particularly obvious feature due to $\mathcal{J}$, c.f. Fig. 4 . The disparity in values of Q_u^+ and Q_u^- near $z^+ = 0$ results from the larger mean sound-speed gradient there as compared to that near $z^- = 1$. The small value of Q_c^- near the surface is due to the nearly negligible value of β near the bottom. Finally, as z^+ and z^- approach $z = a$, the sound-speed gradient and ray curvature approach zero, and consequently β approaches one, causing the increase in all four curves shown near the bottom of Fig. 5 . However, our approximate formulas are not valid for z^+ too close to the axis, because of our use of the stationary-phase method. In particular, given a nondimensional range χ, Eq. (22b) provides a condition $(c_{\mathcal{J}} - c_a) \geq 1/2\ \chi^{-2}$ to be satisfied by the minimum source sound speed. This in turn is a condition on the maximum source depth, which is an upper bound on z^+.

From Fig. 5 , we observe that the Q's are order one in magnitude. Thus, the normalizations of the variance constituents, Eqs. (26), provide appropriate scales for individual turning-point contributions. Suppose now that the brackets in Eqs. (25) are comparable. The relative significance of sound-speed and current effects to the phase variance is determined by the relative magnitudes of $\mathcal{A}_0^2$ and $\mathcal{E}_0^2$. Let the ratio Γ be defined by

$$\Gamma = \mathcal{A}_0^2/\mathcal{E}_0^2 = 2\nu(\mu-\nu)(1-I)/(1+I) \quad . \tag{32}$$

Then, $\Gamma>>1$ (or $\Gamma << 1$) corresponds to sound-speed fluctuations dominating current fluctuations (or vice versa). The value of Γ varies with ν, μ, and I. With respect to the I variation, we note the earlier discussion that Γ is proportional to the ratio of expected potential and kinetic energies. The limiting case I = 0 (or 1) represents internal-wave energy concentrated at the inertial (or far from the inertial) frequency. For I = 0 there are equal amounts of expected energies, while for I = 1 only kinetic energy is present. Thus, for the ν and μ numbers used in Figs. 4 and 5 and values of I = 0, 0.5, and 1, Eq. (32) yields respective values of Γ = 45.5, 15.2, and 0. We conclude that the relative significance of sound-speed and current effects is strongly dependent on a parameter characterizing the frequency distribution of internal-wave energy. The above results are a consequence of our general internal-wave model formulation, c.f. features (3) through (6) of Sec. III, and have been overlooked in previous considerations of internal-wave current effects.[1,2]

There are obvious exceptions to the usefulness of Eq. (32) to determine the relative significance of sound-speed and currents on phase variance. Suppose a ray has a single turning point located deep below the axis. Then, current fluctuations are inevitably dominant, since Q_c^- is nearly zero as in Fig. 5. For reciprocal transmissions, the additive phase variance is always sound-speed dominant, and the excess phase variance always current dominant. As an example of exploiting reciprocal

transmissions, consider a near-grazing ray with $|K^- - K^+| / K^+ << 1$. It follows from Eqs. (25), (27), and (28) that $\mathcal{A}^2 / \mathcal{E}^2$ is approximately Γ. Since $\mathcal{A}^2$ and $\mathcal{E}^2$ are individually observable, the value of I could be estimated if values for μ and ν are known.

To close this section, we compare our phase-variance predictions with the only other calculation for a non-axial ray known to us in the literature, i.e. Eq. (7.4.8) of Ref. 4. That formula corresponds to the particular case in our results of ignoring $\mathcal{E}^2$ in Eq. (20e) and Q_c^- in Eq. (25a). It can be shown that using the parameter values of Ref. 4, our phase-variance prediction differs by the factor $1 + \mathcal{I}[G(z^+)]$. From Fig. 5, it follows that for turning points between the surface and z = b, i.e. $z^* = 850$ m, our prediction is up to 60% greater. For a turning point below z = b, our prediction is up to 30% less. For other parameter values, the predictions can differ by either greater or smaller amounts. In any case, this comparison serves to illustrate a representative numerical difference arising from the features of our environmental-acoustic model.

V. EXPECTED INTENSITY

We investigate the expected value (i.e. the ensemble average) of the acoustic intensity in the presence of a stochastic internal wave field. In the internal wave model, velocity and sound-speed fluctuations are random because of stochastic superposition coefficients.[15] We assume here, as elsewhere (see, for example, Ref. 13) that the coefficients have zero-mean normal distributions.

It follows from Eq. (11b) and Refs. 15 and 31 that the order one phase of any ray at the receiver is also normally distributed. Assuming further that phases of distinct rays at the receiver are mutually independent, the expected intensity, proportional to $\langle \bar{a}^{-2} \rangle$, is given by Eq. (12b). Evaluation of this quantity requires the amplitude, mean travel time, and phase variance for each ray at the receiver, along with the source frequency.

We specify the static sound speed with a bilinear profile, which has been employed previously (see, for example, Refs. 32 and 33) as a convenient mid-ocean model. We take the surface and bottom sound speeds equal, eliminating reflected/refracted rays. Furthermore, we assume that due to bottom and scattering losses, surface-reflected/bottom-reflected rays are of negligible importance to the total received field. Thus, only SOFAR rays are considered, and the ray formulas of Sec. I apply. In particular, Eqs. (10), (11a), and (11d) provide the complete specification of the mean rays. A further simplifying assumption is that the source is placed above the SOFAR axis and the receiver below, such that they are at equal static sound speeds. The analysis of the ray formulas for these static conditions is comprehensively detailed in Sec. I of Ref. 32. We select the numerical values of the bilinear parameters from a recent fit[34] to deep-ocean sound-speed observations: $c_0 = 1543$ m sec^{-1}, $c_a c_0 = 1484$ m sec^{-1}, $D = 4900$ m, and $aD = 1100$ m.

For the phase variance, we wish to apply the formulation of Secs. III and IV. The principal restriction on those results is Eq. (22b), derived from the condition $\kappa \geq 1$. For the bilinear profile and source at nondimensional depth $d < a$, Eq. (22b)

becomes

$$\chi \geq \{a/[2(1-c_a)(a-d)]\}^{1/2} \quad . \tag{33}$$

Using our profile parameters and dimensional source depths dD of 100, 400, 700, and 1000 m, Eq. (33) is satisfied for ranges greater than about 19, 22, 29, and 60 km, respectively. As the source approaches the axis, larger ranges are needed to eliminate "near-axial" rays. However, as suggested by the numerical examples for shallow or moderate source depths, the restriction is not severe for the bilinear profile. This results mathematically because Eq. (33) behaves like $(a-d)^{-1/2}$ as $d \to a$, whereas for differentiable profiles, the analogous expression grows faster, like $(a-d)^{-1}$.

To specify the variance constituents, Eqs. (25), we first require the distribution of Brunt-Vaisala frequency N(z). For our consistent environmental-acoustic model, specification of the static sound speed determines N(z), as discussed in Sec. II. By Eqs. (14b) - (14d), the bilinear profile leads to an N(z) which is bi-constant (two discontinuous vertical line segments). We choose the previous numbers $\mu = 11.6$ and $\nu = 9.1$, to facilitate comparisons with earlier results; also, these values correspond to a smooth static profile in Sec. IV that approximates the observations to which the bilinear profile was fit in Ref. 34. Thus, we obtain Brunt-Vaisala frequencies of 4.0 cyc h^{-1} (or 0.4 cyc h^{-1}) between surface and axis (or axis and bottom). Also, we choose the velocity scale $U_0 = 2.72$ cm sec^{-1} as in Sec. III.

The turning-point contributions to the phase variance are specified by Eqs. (27) if we select a model for $H(j/j_*)$, for

which we use Eq. (29a). In Fig. 6, we graph the turning-point contributions versus dimensionless upper turning depth for the bi-constant N(z) and the value $j_* = 3$. It is important to note that the curves in Fig. 6 enjoy the same features as those in Fig. 5 for the exponential N(z), with one exception. The curves in Fig. 6 do not show the sharp increase as z^+ approaches a. This is because the increase results from profile curvature, which is absent from the bilinear model. Thus, in order that the bi-constant and exponential cases have similar turning-point contributions, we want ray upper turning depths to avoid depths influenced by profile curvature. One way to assure this is to place the source sufficiently far from the axis, for example, at a dimensional depth of 400 m shown on Fig. 6 as a horizontal line (this particular value was also used in Ref. 34). All upper turning points necessarily lie above the source depth. Moreover, comparison of corresponding curves in Fig. 5 and 6 show that the numerical values above this source depth are quite similar.

Before computation of the expected intensity, it is appropriate to check an interfacing trapezoid for our application. A proper choice for the error parameter γ of Sec. II is $N_0/\pi = 0.10$, which is the order to which the WKB(J) solutions for the internal-wave model are obtained in Ref. 15. It happens that the WKB(J) solutions are exact for the bi-constant N(z). However, in the stationary-phase approximation of ϕ in Sec. IV, terms of this order are ignored. Thus, we have an example of the situation noted just below Eq. (18b), and our choice $\gamma = N_0/\pi > \Delta$ is justified. We also select $\varepsilon = \gamma$ for our tolerable acoustic error

(approximately ten per cent). From Eqs. (16) and (17), we may construct an interfacing trapezoid. We do not present its graph, because for the parameter values specified in this section, its three nonvertical sides are quantitatively very close to those of the $U_0 = 3$ cm sec^{-1} trapezoid in Fig. 3. Its leftmost (vertical) boundary is the line $\chi = 4.4$, corresponding to equality in Eq. (33) and representing a stronger condition than was required in Sec. II. Therefore, our selection of acoustic operating conditions must lie within this trapezoid. In addition, we desire that the range interval lie in a "stability region" for the static bilinear profile.[34] Such requirements are satisfied by the choices $f_0 = 100$ H_z and R_0 between 200 and 222 km, which we will use for subsequent calculations. We note that in this range interval, four SOFAR rays intercept the receiver, each with seven axis crossings.

We turn to investigation of the intensity. In order to illustrate the nature of internal-wave effects, we introduce the following notation:

$$\bar{\alpha}_I^{-2} = \sum_n A_{(n)}^2 \quad , \tag{34a}$$

$$\bar{\alpha}_c^{-2} = \bar{\alpha}_I^{-2} + \sum_{\substack{n \\ n \neq m}} \sum_m A_{(n)} A_{(m)} \cos\left[\omega(T_{(n)} - T_{(m)})\right] \quad , \tag{34b}$$

and

$$\bar{\alpha}_M^{-2} = \bar{\alpha}_I^{-2} + \sum_{\substack{n \\ n \neq m}} \sum_m A_{(n)} A_{(m)} \quad . \tag{34c}$$

As mentioned in Sec. I, $\bar{\alpha}_I^{-2}$ (or $\bar{\alpha}_c^{-2}$) is proportional to the incoherent (or coherent) intensity, and is the limit of $\langle \bar{\alpha}^{-2} \rangle$ as

the phase variance on each ray approaches infinity (or zero). From Eq. (34b), it follows that α_M^{-2} in Eq. (34c) is proportional to the maximum value of the coherent intensity. We note that α_M^{-2} is the square of the sum of the static ray amplitudes.

Figure 7 is a graph versus dimensional range of Eqs. (34) in dB relative to a sphere at dimensionless radius r, as discussed prior to Eq. (7a). In addition, $\langle \bar{\alpha}^{-2} \rangle$ from Eq. (12b) is shown in dB for internal-wave parameters I = 0.5 and $j_* = 3$. Calculations were made using a range increment of 0.2 km. The comparative magnitudes of variations are as follows. The drop in incoherent intensity over about 20 km of range is approximately 7 dB. The difference between incoherent intensity and the maximum coherent intensity is about 6 dB at each R_0. The difference between the coherent and incoherent intensities varies from about -10 dB to 6 dB, except for one deep fade of at least 18 dB near 212.6 km. The difference between the expected and incoherent intensities varies from about -3 dB to 4 dB. We conclude that the deviations from both coherent and incoherent intensities produced by internal waves can be very significant. Although at isolated ranges all three intensities agree, neither coherent nor incoherent intensities provides an accurate picture of range variations in the presence of internal waves. For example, the depth of fades is curtailed by the internal waves. We note that the value of the expected intensity at each range lies between the coherent and incoherent intensities. From Eq. (12b), this occurs because all rays have approximately the

same phase variance for $I = 0.5$ and $j_* = 3$.

We now consider variations in the expected intensity resulting from changes in the internal-wave parameters. The internal-wave energy-density spectral functions $B(\hat{\omega})$ and $H(j/j_*)$ are useful representations of observations. However, at present there is no certainty, based on dynamical principles, of the correct form or parametric values for the spectra,[24] in any given ocean region. We regard variations in the parameters j_* and I as modeling certain types of changes in the internal-wave field between different oceanic regions, or between different times in the same region. Indeed, changes in these characteristics have evolved with the acquisition of new data.[10, 29]

In Fig. 8, we graph the expected intensity relative to the incoherent intensity in dB versus range for $I = 0.5$ and $j_* = 0, 3$, and 7. Thus, the solid curve in Fig. 8 represents the difference between the two solid curves in Fig. 7 . We note the increased variation of the expected intensity about the incoherent as j_* increases. For $j_* = 0$, 3, and 7, intensity varies by approximately 2.5, 7, and 9 dB, respectively, as R_0 changes over the interval shown. These results are consistent with increased mode interaction, mentioned in connection with J_* in Sec. IV.

We show similar curves with $j_* = 3$ and $I = 0$, 0.5, and 1 in Fig. 9 , where the solid curve has the same meaning as in Fig. 8. Again, increased fluctuation of the expected intensity about the incoherent occurs as the internal-wave parameter increases. For $I = 0$, 0.5, and 1, intensity varies by about 3, 6.5, and 21 dB, respectively, as R_0 changes. The behavior of the expected intensity with I is interpreted by considering the maximum of a_0^2 and $\mathcal{E}_0^2$ as an appropriate scale for σ^2. From Eqs. (26), it can be shown

that for $2\nu(\mu-\nu) > 1$, this maximum decreases as I increases. The fluctuations become very dramatic as I approaches one, reaching nearly the size of those of the coherent intensity about the incoherent. Thus, mean intensity is even more sensitive to variations in I than j_*. We note that variations with range in received intensity have been studied previously; recent examples include Ref. 33 and 35. However, to the authors' knowledge, the explicit effects of internal waves, and of course variations in the internal-wave field, on multipath expected intensity have not been considered previously.

VI. SUMMARY

The two principal purposes of this paper are to formulate a consistent environmental-acoustic model for a deep moving ocean and to apply the model to investigate effects of a stochastic internal-wave field on sound propagation. Equations of the model are approximately solved using a type of WKB(J) expansion in the non-dimensional frequency ω. Explicit connection is made between environmental and acoustic parameters by assuming that $F = M\omega$, where M is the Mach number, is asymptotically order one with respect to ω. Other assumptions include considering only SOFAR rays which are regularly perturbed by order M sound-speed and velocity changes. Our results modify traditional ray-theory formulas for the order one phase, but not the amplitude, of a single ray. Both deterministic and stochastic velocity and sound-speed perturbations may be treated by our model. As an example of an important statistic of the received acoustic field, we present a formula for the

expected multipath intensity, assuming stochastic ray phases which are both independent and Gaussian.

Interfacing conditions between acoustic and hydrodynamic models are stated and motivated. These conditions depend on the values selected for the variable scales, such as characteristic velocity U_0 and length X_0. In this paper, the choice for X_0 is ocean depth, but our techniques may be applied to other types of problems, for which different scales are appropriate. Interfacing trapezoids, which bound permissible regions of transmission range R_0 and CW frequency f_0, are constructed and interpreted. As one example, the trapezoid in Fig. 2 for $U_0 = 3$ cm sec^{-1} indicates that for $R_0 = 200$ km, the permissible frequency band is about 30 to 560 Hz. To our knowledge, the role of interfacing in providing such constraints has been overlooked previously. A consistent and general relation between the Brunt-Vaisala frequency and static sound-speed distribution is also developed. Significant simplification of the fluctuation-dependent ray phase is obtained through our consistent approach.

We apply our model to the derivation of formulas for ray phase variance in the presence of a stochastic internal-wave field. The phase variance is a fundamental statistic for both total-field intensity calculations and reciprocal acoustic transmissions. To describe the internal-wave fluctuations, we use a consistent model previously published by the authors. Advantages of this model include its incorporation of vertical mode structure and its independence of specific internal-wave spectral functions and static-state distributions. The phase variance is found to split into two constituents, depending on the velocity and sound-speed fluctuations individually.

Approximate evaluation of our formulas for the constituents is feasible for two classes of rays, one including axial and "near-axial" rays and another for which the rays possess relatively significant variation in depth over transmission range. We evaluate the constituents for the second class using a stationary phase approximation. Justification for this procedure is a direct consequence of our consistent model formulation. Moreover, the consistency and generality of our analysis enables us to obtain many new results and predictions for the variance constituents. For example, sound-speed (velocity) contributions to the variance are apportioned according to the amount of internal-wave expected potential (kinetic) energy. The relative significance of these contributions is shown to be strongly dependent on a parameter I, which characterizes the frequency distribution of internal-wave energy. Further, the internal-wave mode number spectrum is shown to significantly modify the depth dependence of the variance constituents. The degree of influence depends on model parameters and ray turning depths; in one case which can be compared with previously-published results, our predictions range from 60% greater to 30% less.

We apply our phase variance results to the evaluation of expected total-field intensity in an ocean modeled by a bilinear static sound-speed distribution. Consistency requirements are used to determine an appropriate bi-constnat Brunt-Vaisala frequency and to suggest feasible values for propagation parameters. We show that deviations from both coherent and incoherent intensities produced by internal waves can be very significant, and that neither of these intensities provides an accurate picture of the variations

with R_0 in the presence of internal waves. The effects of variations of the internal-wave parameters I and j_* are examined and interpreted. Increased fluctuations of the expected intensity about the incoherent are observed as either of these parameters increase. For the cases we examined, the magnitudes of these fluctuations can be very dramatic, as high as 21 dB over the interval of R_0 values considered.

REFERENCES

1. W. H. Munk and F. Zachariasen, Stanford Research Institute, Menlo Park, Tech. Rep. No. JSR-77-21 (unpublished).

2. P. F. Worcester, J. Acoust. Soc. Am. 62, 895-905 (1977).

3. R. P. Porter, R. C. Spindel, and R. J. Jaffee, J. Acoust. Soc. Am. 56, 1426-1436 (1974).

4. S. M. Flatte, R. Dashen, W. Munk, and F. Zachariasen, Stanford Research Institute, Menlo Park, Tech. Rep. No. JSR-76-39 (unpublished).

5. W. H. Munk and F. Zachariasen, J. Acoust. Soc. Am. 59, 818-838 (1976).

6. Y. J. F. Desaubies, J. Acoust. Soc. Am. 60, 795-800 (1976).

7. W. Jobst and J. Clark, J. Acoust, Soc. Am. 61, 688-693 (1977).

8. W. Jobst, X. Zabalgogeazcoa, and N. L. Weinberg, J. Acoust. Soc. Am. 61, 1163-1168 (1977).

9. B. J. Uscinski, "Sound propagation through internal waves in the ocean", (unpublished).

10. C. J. R. Garrett and W. H. Munk, Geophys. Fluid Dyn. 2, 225-264 (1972).

11. F. Dyson, W. Munk, and B. Zetler, J. Acoust. Soc. Am. 59, 1121-1133 (1976).

12. R. P. Porter and R. C. Spindel, J. Acoust. Soc. Am. 61, 943-958 (1977).

13. S. M. Flatte and F. D. Tappert, J. Acoust. Soc. Am. 58, 1151-1159 (1975).

14. L. B. Dozier and F. D. Tappert, J. Acoust. Soc. Am. 63, 353-365 (1978).

15. J. G. Watson, W. L. Siegmann, and M. J. Jacobson, J. Acoust. Soc. Am. 61, 716-726 (1977).

16. E. U. Condon and H. Odishaw, Eds. Handbook of Physics (McGraw-Hill, New York, 1958), p. 3-113.

17. P. L. Chow, SIAM Rev. 17, 57-81 (1975).

18. A. H. Nayfeh, Perturbation Methods (Wiley, New York, 1973), Ch. 7.

19. J. T. Warfield and M. J. Jacobson, J. Acoust. Soc. Am. 50, 342-347 (1971).

20. J. A. Neubert, J. Acoust. Soc. Am. 51, 310-322 (1972).

21. J. G. Watson, W. L. Siegmann, and M. J. Jacobson, J. Acoust. Soc. Am. 60, 355-364 (1976).

22. R. N. Baer and M. J. Jacobson, J. Acoust. Soc. Am. 55, 1178-1189 (1974).

23. W. H. Munk, J. Acoust. Soc. Am. 55, 220-226 (1974).

24. O. M. Phillips, The Dynamics of the Upper Ocean, 2nd ed. (University Press, Cambridge, 1977), Ch. 5.

25. R. B. Lindsay, Mechanical Radiation (McGraw-Hill, New York, 1960), pp. 41-47.

26. C. C. Lin and L. A. Segel, Mathematics Applied to Deterministic Problems in the Natural Sciences (Macmillan, New York, 1974), pp. 213-214.

27. J. B. Keller, Proceedings of Symposia in Applied Mathematics, Vol. 13 (American Mathematical Society, Providence, 1962), pp. 227-246.

28. E. T. Copson, Asymptotic Expansions (Cambridge University, London, 1965), Ch. 4.

29. J. L. Cairns and G. O. Williams, J. Geophys. Res. 81, 1943-1950 (1976).

30. Handbook of Mathematical Functions, ed. by M. Abramowitz and I. A. Stegun (Dover, New York, 1965), p. 259.

31. T. T. Soong, Random Differential Equations in Science and Engineering (Academic Press, New York, 1973), p. 112.

32. R. N. Baer and M. J. Jacobson, J. Acoust. Soc. Am. 57, 569-576 (1975).

33. G. M. Jacyna and M. J. Jacobson, J. Acoust. Soc. Am. 63, 1353-1364 (1978).

34. G. M. Jacyna and M. J. Jacobson, J. Acoust. Soc. Am. 61, 1153-1162 (1977).

35. J. A. Neubert, J. Acoust. Soc. Am. 62, 326-334 (1977).

FIGURE LEGENDS

FIG. 1. Coordinate system, source location, and a ray path.

FIG. 2. Interface trapezoids in frequency f_0 (Hz) and range R_0 (km) plane for error paramters $\gamma = \Delta$ and $\varepsilon = \Delta$, and characteristic velocities U_0 = 1, 3, and 10 cm sec^{-1}.

FIG. 3. Interface trapezoids in frequency f_0 (Hz) and range R_0 (km) plane for error paramters $\gamma = \Delta^{1/2}$ and $\varepsilon = \Delta^{1/2}$, and characteristic velocities U_0 = 1, 3, and 10 cm sec^{-1}.

FIG. 4. Dimensionless vertical-structure function $\mathcal{G}[G(z)]$ versus dimensionless depth z for exponential Brunt-Vaisala frequency and $j_* = 0$, 3, and 7.

FIG. 5. Dimensionless ray-phase turning-point contributions Q_c^+ and Q_u^+ versus dimensionless upper-turning depth z^+ for exponential Brunt-Vaisala frequency.

FIG. 6. Dimensionless ray-phase turning-point contributions Q_c^+ and Q_u^+ versus dimensionless upper-turning depth z^+ for bi-constant Brunt-Vaisala frequency.

FIG. 7. Relative intensity (dB) versus range R_0 (km) for bilinear static sound speed and f_0 = 100 Hz, showing incoherent, coherent, maximum coherent, and expected (I = 0.5 and $j_* = 3$) intensities.

FIG. 8. Expected intensity relative to incoherent intensity (dB) versus range R_0 (km) for I = 0.5 and $j_* = 0$, 3, and 7.

FIG. 9. Expected intensity relative to incoherent intensity (dB) versus range R_0 (km) for $j_* = 3$ and I = 0, 0.5, and 1.

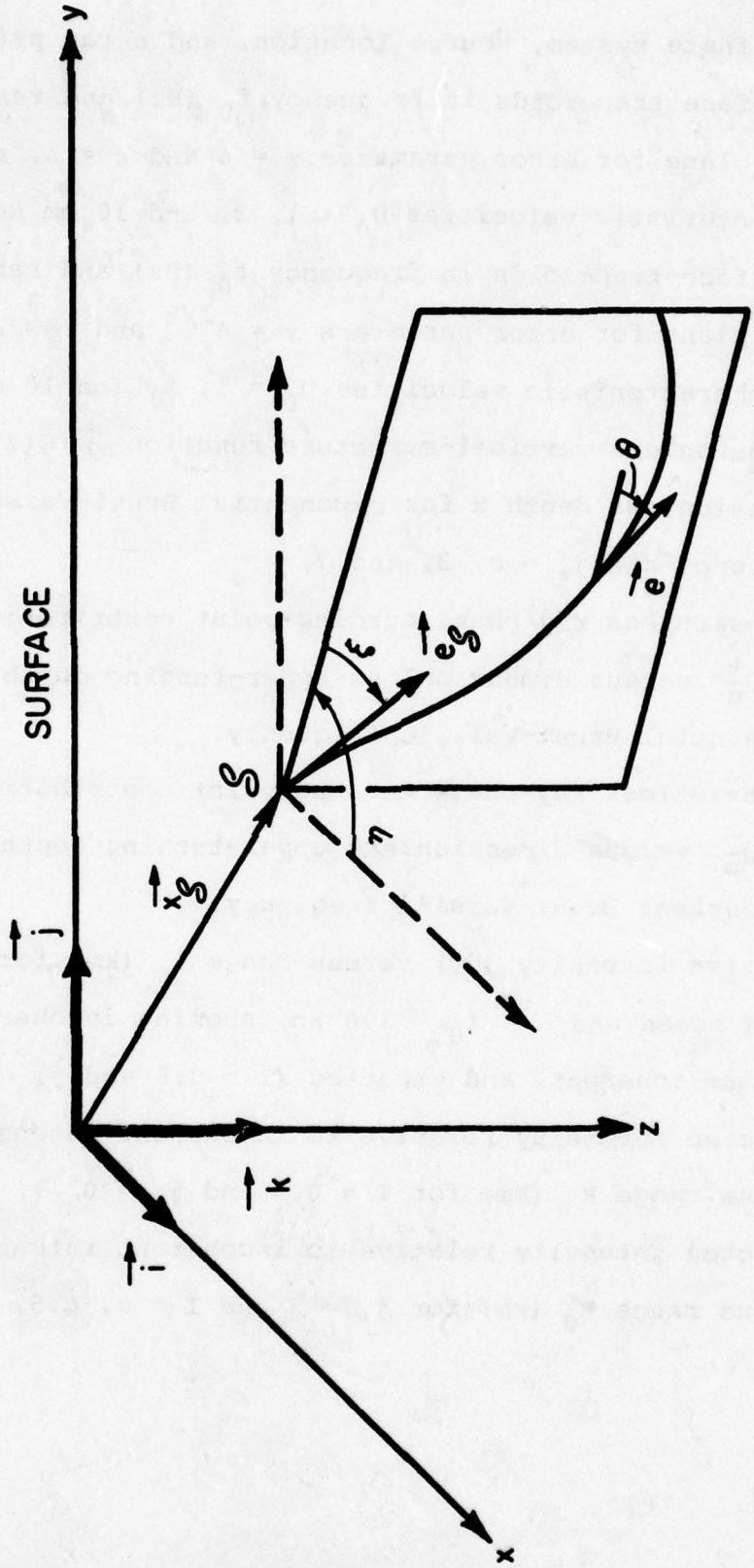

FIGURE 1

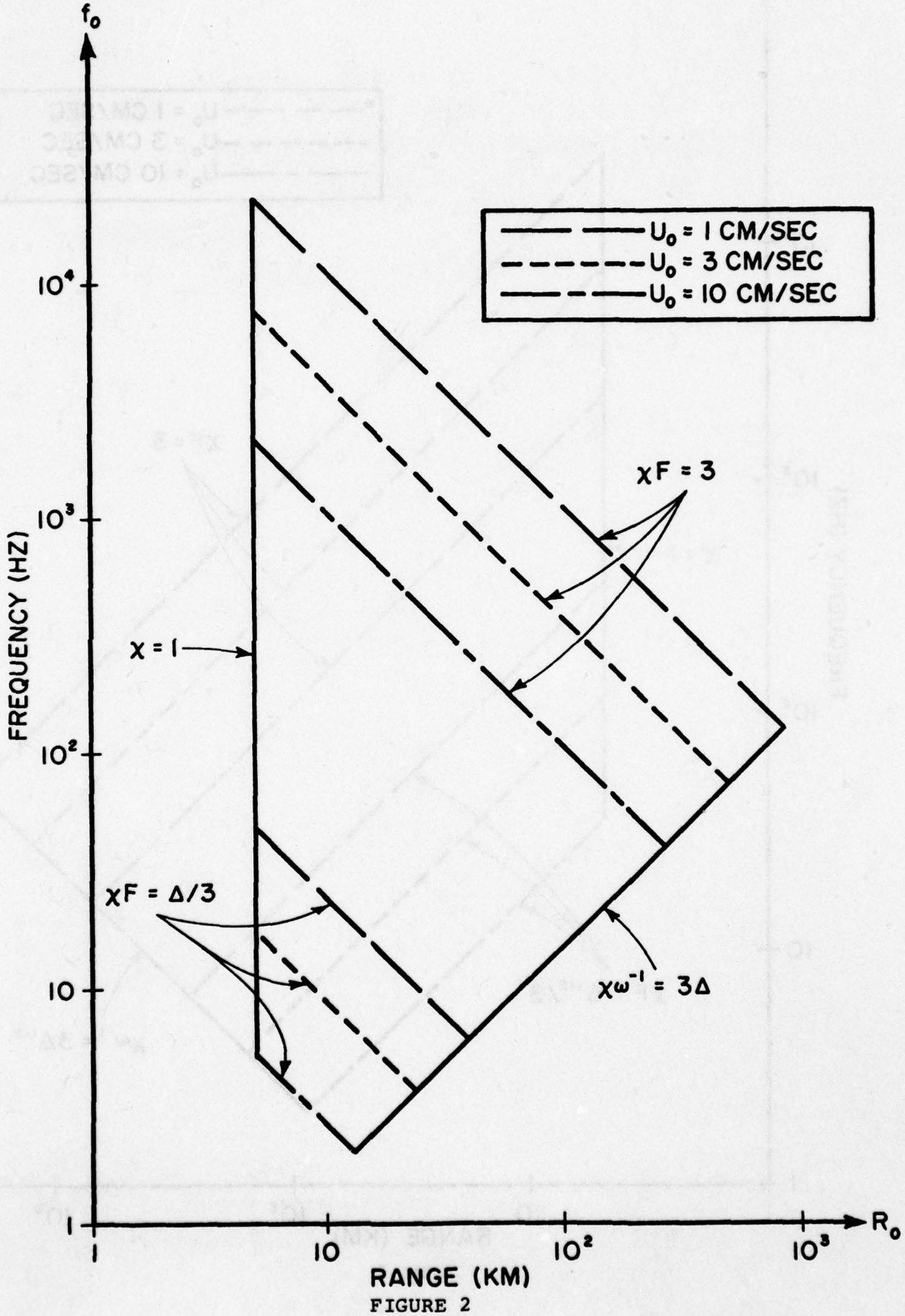
f_o
U_o = 1 CM/SEC
U_o = 3 CM/SEC
U_o = 10 CM/SEC
10^4
10^3
10^2
10
1
FREQUENCY (HZ)
$\chi F = 3$
$\chi = 1$
$\chi F = \Delta/3$
$\chi\omega^{-1} = 3\Delta$
1
10
10^2
10^3
R_o
RANGE (KM)

FIGURE 2

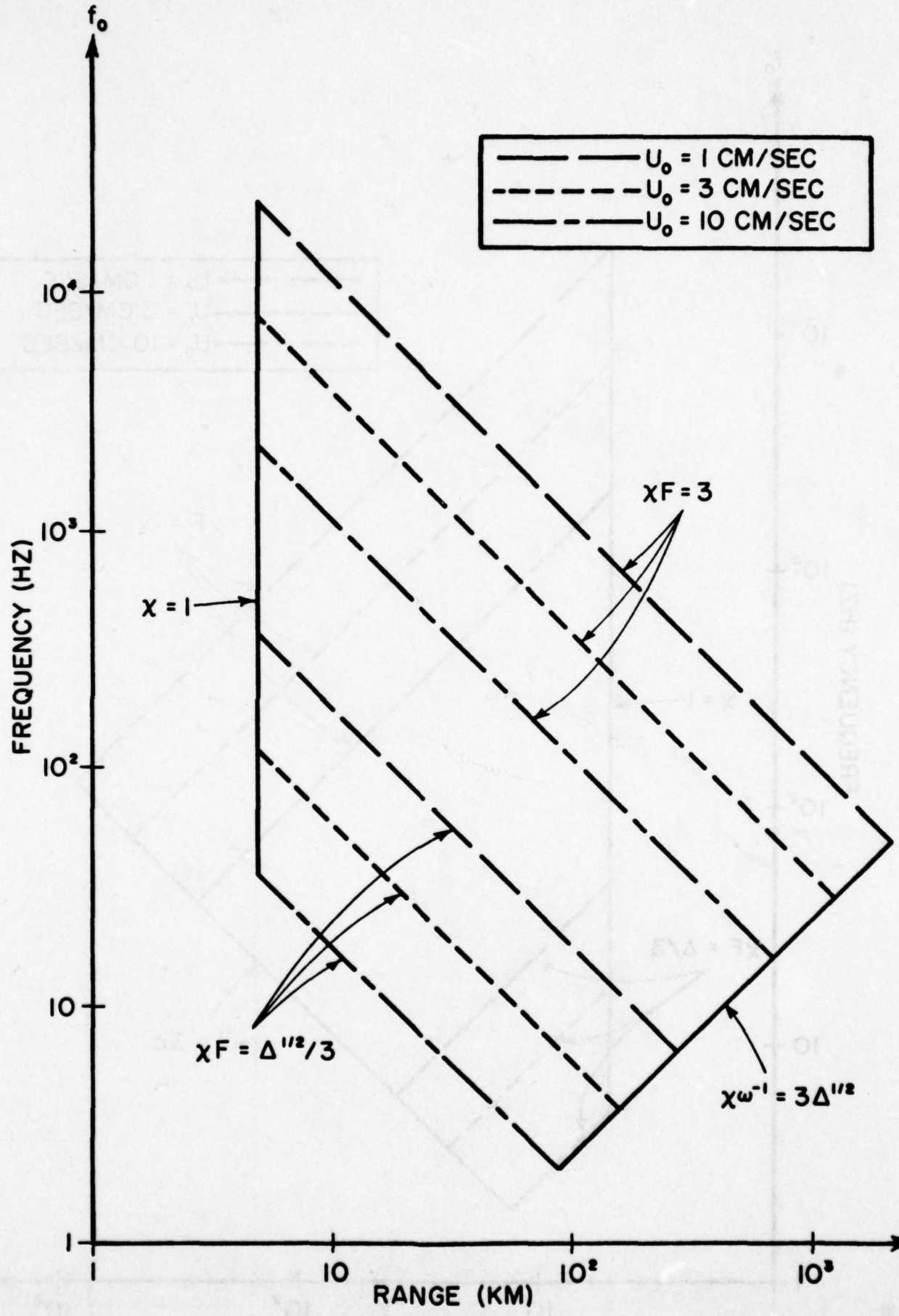
f_0
U_0 = 1 CM/SEC
U_0 = 3 CM/SEC
U_0 = 10 CM/SEC
10^4
10^3
10^2
10
1
FREQUENCY (HZ)
$\chi F = 3$
$\chi = 1$
$\chi F = \Delta^{1/2}/3$
$\chi\omega^{-1} = 3\Delta^{1/2}$
1
10
10^2
10^3
R_c
RANGE (KM)

FIGURE 3

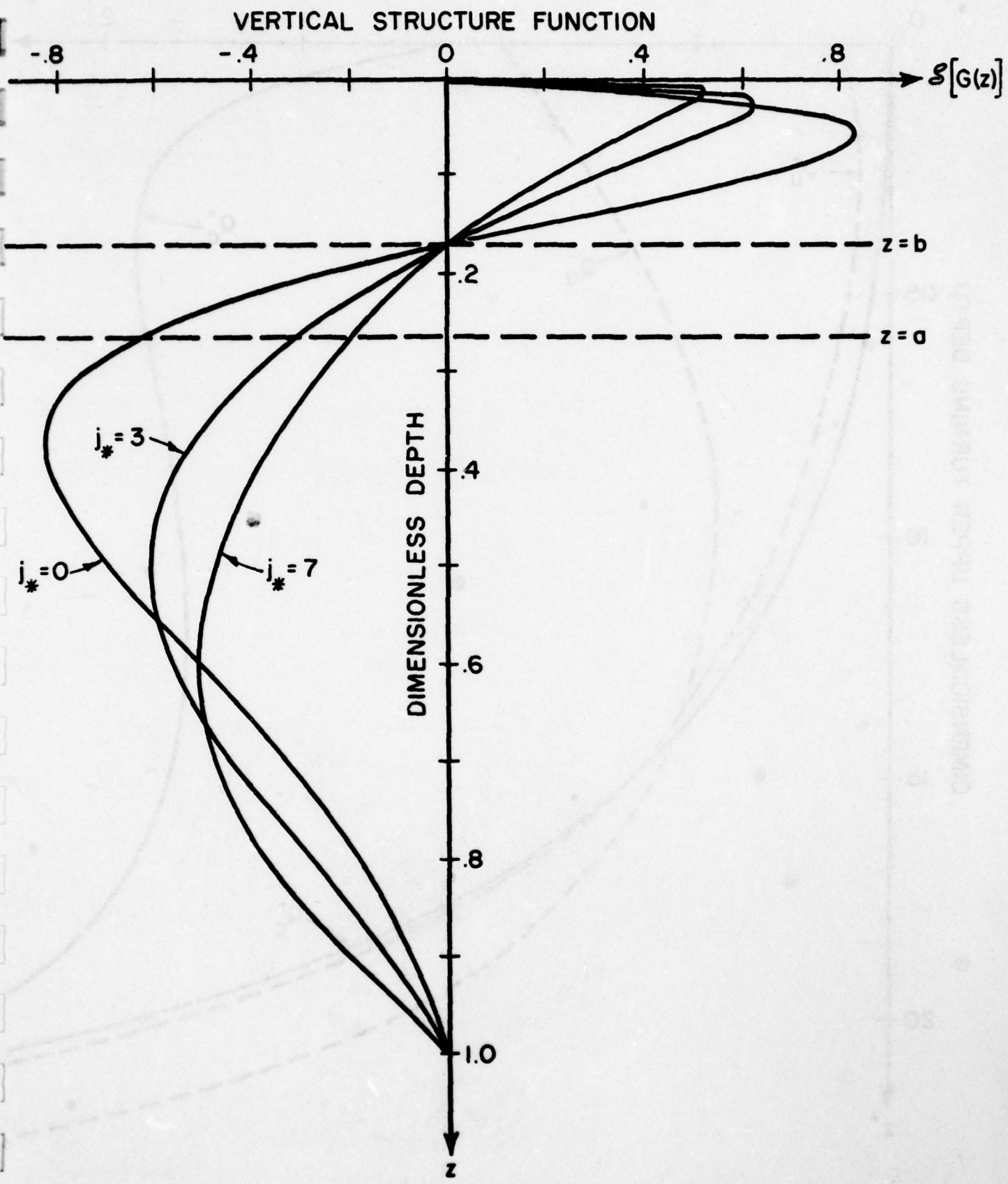
VERTICAL STRUCTURE FUNCTION
-.8
-.4
0
.4
.8
$\mathcal{S}[G(z)]$
z = b
z = a
.2
.4
.6
.8
1.0
DIMENSIONLESS DEPTH
$j_* = 3$
$j_* = 0$
$j_* = 7$
z

FIGURE 4

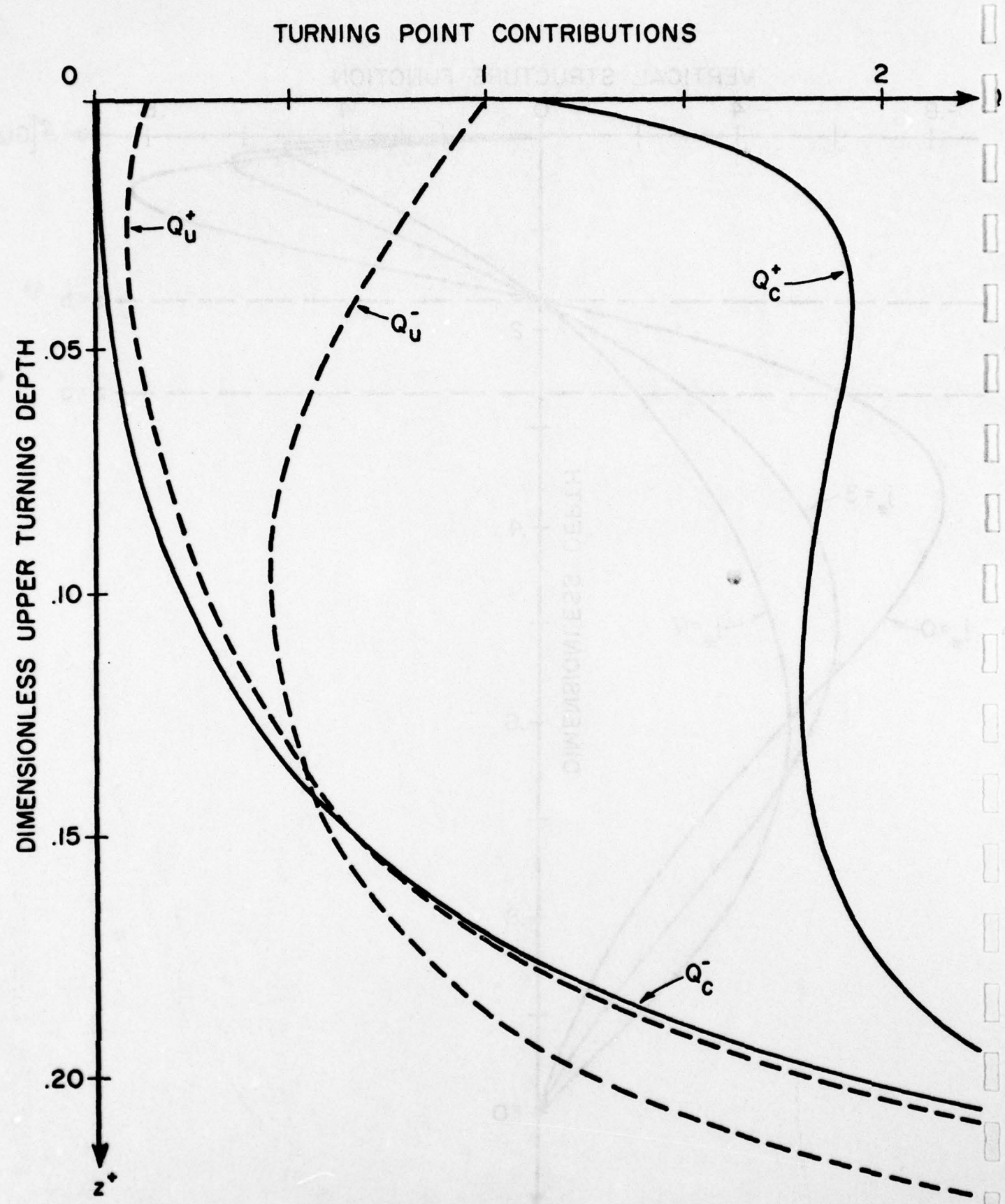
TURNING POINT CONTRIBUTIONS
0
1
2
Q_u^+
Q_u^-
Q_c^+
Q_c^-
DIMENSIONLESS UPPER TURNING DEPTH
.05
.10
.15
.20
z^+

FIGURE 5

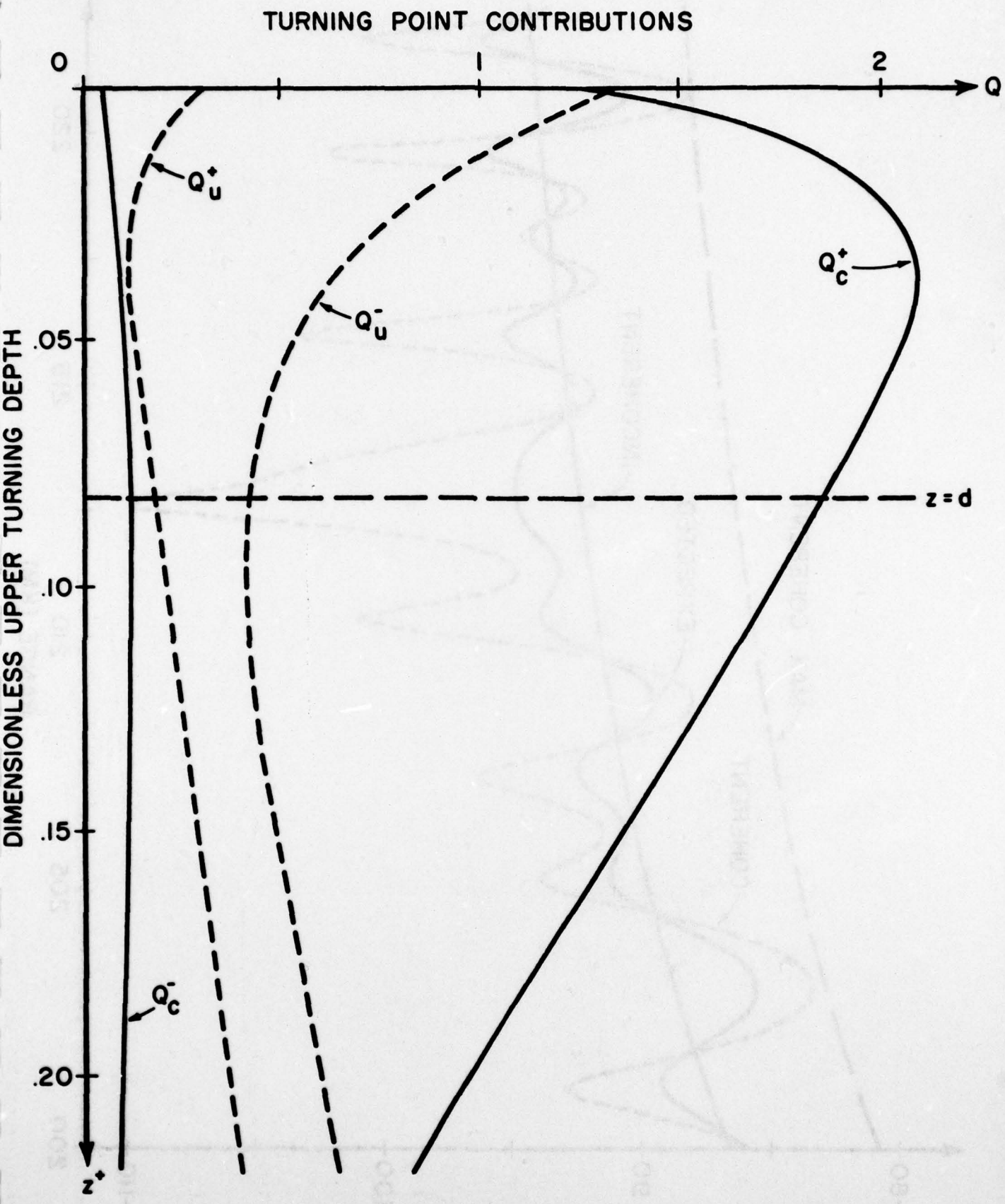
TURNING POINT CONTRIBUTIONS
0
1
2
Q
Q_u^+
Q_u^-
Q_c^+
Q_c^-
z = d
.05
.10
.15
.20
DIMENSIONLESS UPPER TURNING DEPTH
z^+

FIGURE 6

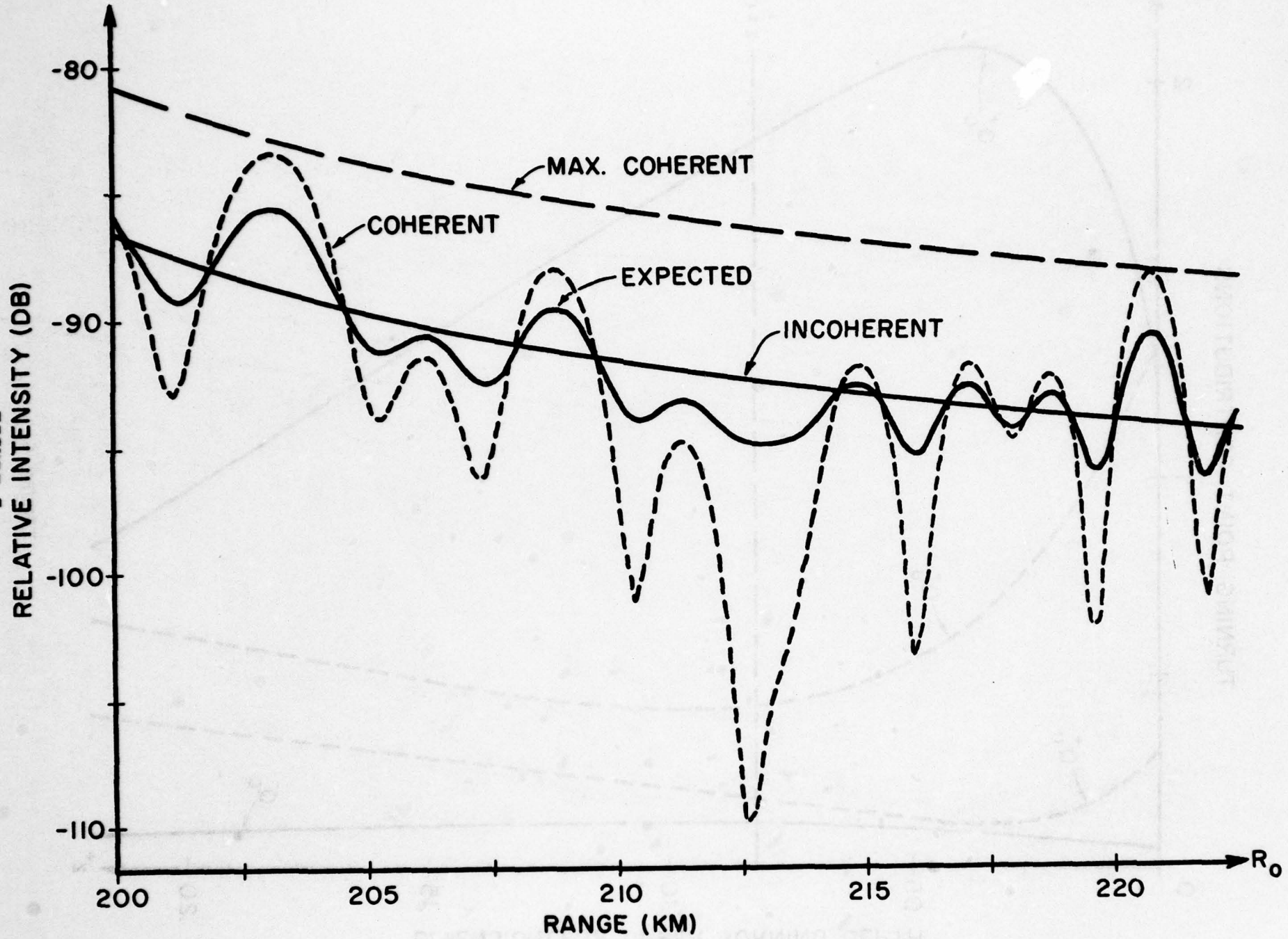
-80
-90
-100
-110
MAX. COHERENT
COHERENT
EXPECTED
INCOHERENT
RELATIVE INTENSITY (DB)
200
205
210
215
220
R_o
RANGE (KM)

FIGURE 7

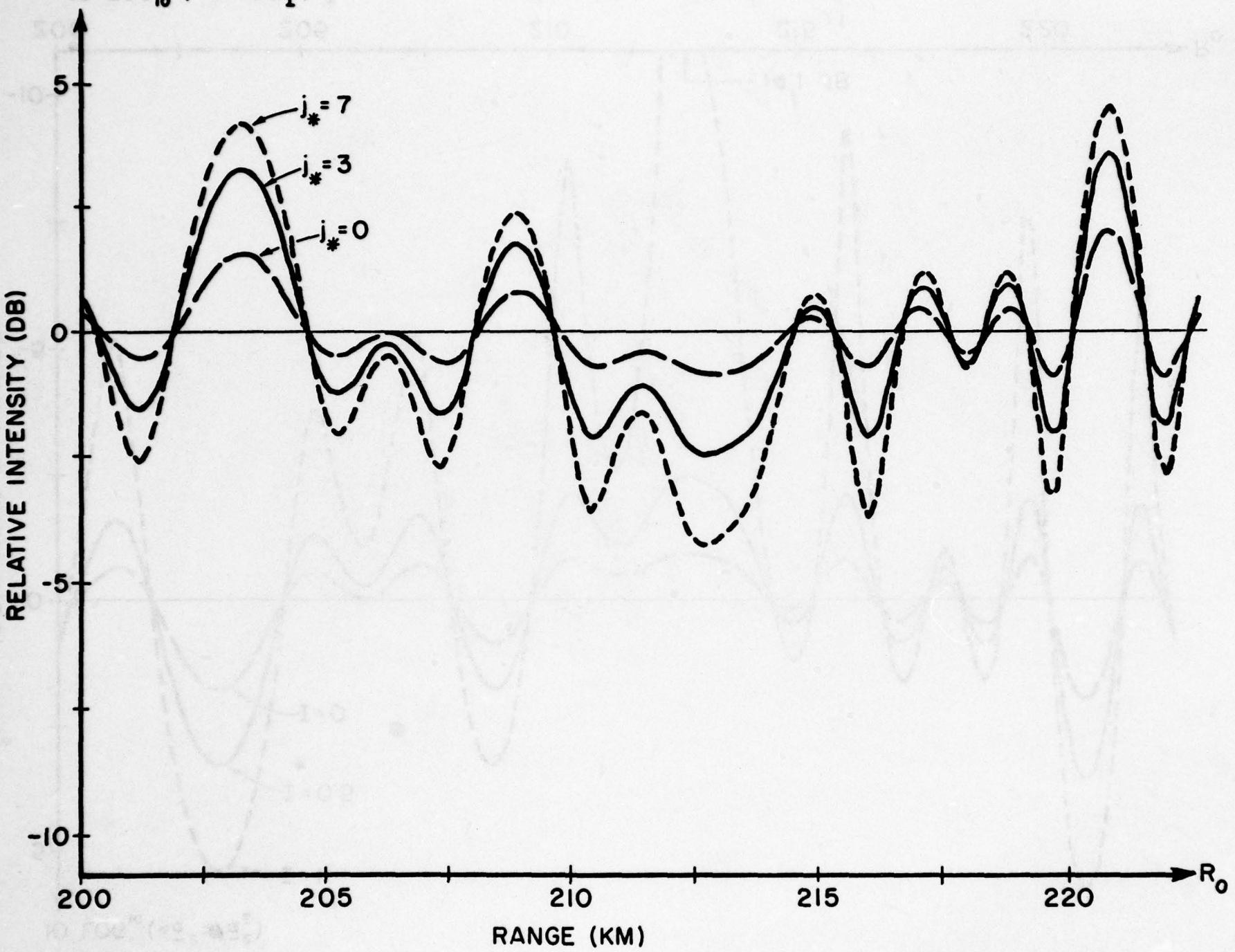
10 LOG10 (<ā²> / ā²I)
5
0
-5
-10
j* = 7
j* = 3
j* = 0
RELATIVE INTENSITY (DB)
200
205
210
215
220
R0
RANGE (KM)

FIGURE 8

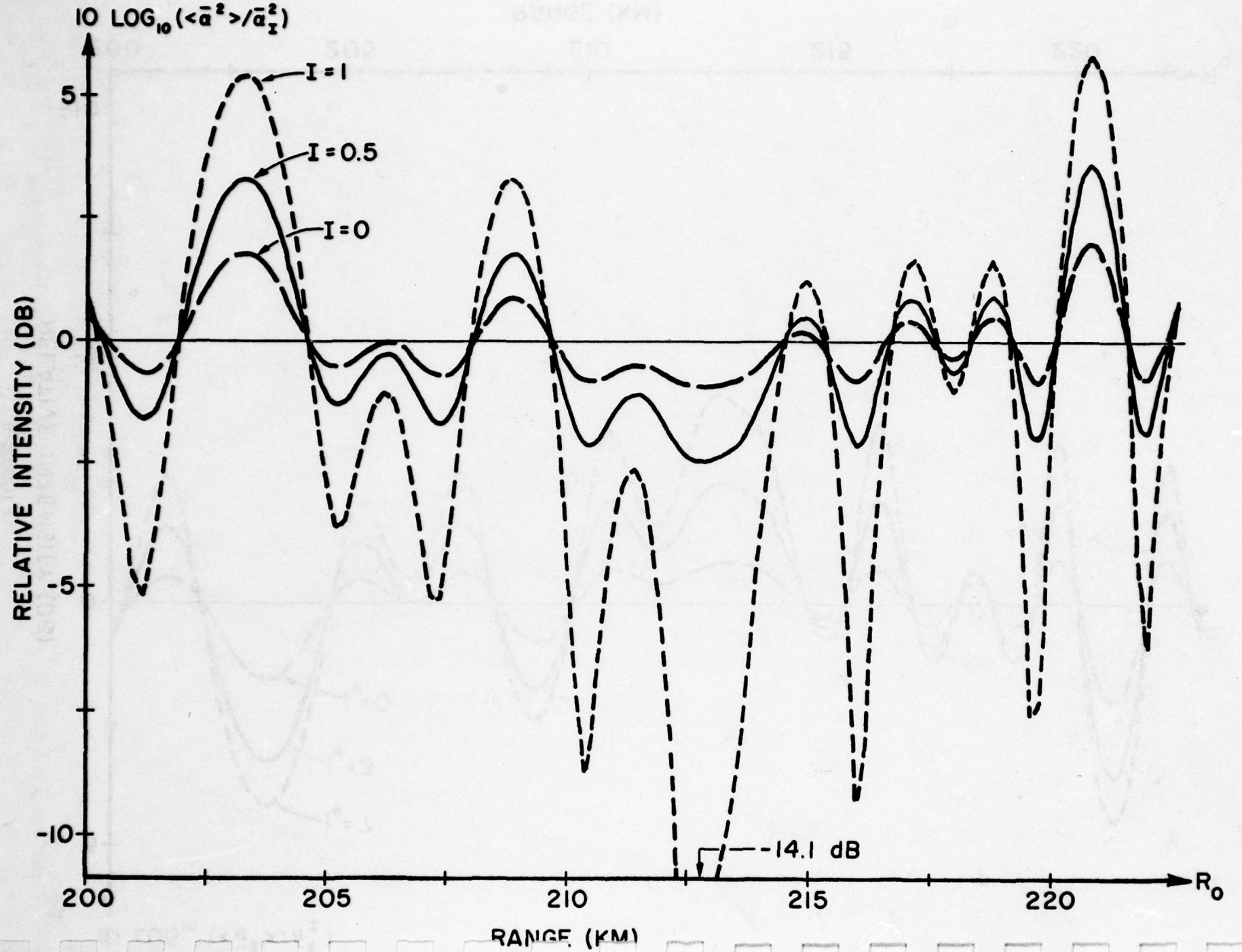
10 LOG10(<ā²>/ā²I)
I = 1
I = 0.5
I = 0
5
0
-5
-10
RELATIVE INTENSITY (DB)
-14.1 dB
200
205
210
215
220
R0
RANGE (KM)

FIGURE 9

DISTRIBUTION LIST

Office of Naval Research (Code 222) (Code 102-OS) (Code 480) Department of the Navy Arlington, Virginia 22217		2 1 1
Director Naval Research Laboratory Technical Information Division Washington, D. C. 20375		6
Director Office of Naval Research Branch Office 1030 East Green Street Pasadena, California 91106		1
Office of Naval Research San Francisco Area Office 760 Market Street - Room 447 San Francisco, California 94102		1
Director Office of Naval Research Branch Office 495 Summer Street Boston, Massachusetts 02210		1
Office of Naval Research New York Area Office 207 West 24th Street New York, New York 10011		1
Director Office of Naval Research Branch Office 536 South Clark Street Chicago, Illinois 60605		1
Code 102 IP Office of Naval Research Arlington, Virginia 22217	(Uncl.) (No Class. Reports)	8
Commander Naval Ordnance Laboratory Acoustics Division White Oak Silver Spring, Maryland 20910 ATTN: Dr. Zaka Slawsky		1

DISTRIBUTION LIST - 2

Officer in Charge Annapolis Laboratory Naval Ship Research and Development Center Annapolis, Maryland 21402	1
Commander Naval Sea Systems Command Code SEA 037 Washington, D. C. 20362	1
Commander Naval Sea Systems Command Washington, D. C. 20362 ATTN: Mr. Carey D. Smith (Code SEA 06H1) CDR Bruce Gilchrist (Code SEA 06H2)	 1 1
Officer in Charge Pasadena Laboratory Naval Undersea Center 3202 East Foothill Boulevard Pasadena, California 91107	1
Commanding Officer Fleet Numerical Weather Central Monterey, California 93940	1
Defense Documentation Center Cameron Station Alexandria, Virginia 22314	20
Chief of Naval Material Department of the Navy Washington, D. C. 20360 ATTN: Mr. James Probus (Acting Director of Navy Laboratories)	1
Office of The Secretary of Defense DDR&E Pentagon, Room 3E1040 Washington, D. C. 20350 ATTN: Mr. Allan D. Simon	1
Commander Naval Electronic Systems Command Washington, D. C. 20360 ATTN: CAPT J. Bajus (NAVELEX 03) CDR A. Miller (NAVELEX 320)	 1 1

DISTRIBUTION LIST - 3

Chief of Naval Operations — 1
Department of the Navy
Pentagon, Room 5B718
Washington, D. C. 20350
ATTN: CAPT Robert B. Brunsted

Commander — 1
Naval Ship Research and Development Center
Bethesda, Maryland 20034
ATTN: Mr. Craig Olson

Chief of Naval Operations — 1
Department of the Navy
Pentagon, Room 4C559
Washington, D. C. 20350
ATTN: CDR A. H. Gilmore

Commander
Naval Undersea Center
San Diego, California 92132
ATTN: Dr. Dan Andrews — 1
Mr. Henry Aurand — 1

Chief Scientist — 1
Navy Underwater Sound Reference Division
P. O. Box 8337
Orlando, Florida 32806

Officer in Charge — 1
New London Laboratory
Naval Underwater Systems Center
New London, Connecticut 06320

Commander — 1
Naval Air Development Center
Warminster, Pennsylvania 18974

Commander — 1
Naval Ship Research and Development Center
Bethesda, Maryland 20034

Superintendent — 1
Naval Postgraduate School
Monterey, California 93940

Commanding Officer — 1
Naval Coastal Systems Laboratory
Panama City, Florida 32401

Commanding Officer — 1
Naval Underwater Systems Center
Newport, Rhode Island 02840

DISTRIBUTION LIST - 4

Superintendent
Naval Academy
Annapolis, Maryland 21402 — 1

Commanding Officer
Naval Intelligence Support Center
4301 Suitland Road
Washington, D. C. 20390
ATTN: Dr. Johann Martinek — 1
Mr. E. Bissett — 1

Commander
Naval Sea Systems Command
Code SEA 03E
Washington, D. C. 20362 — 1

Dr. Melvin J. Jacobson
Rensselaer Polytechnic Institute
Troy, New York 12181 — 1

Dr. Charles Stutt
General Electric Company
P. O. Box 1088
Schenectady, New York 12301 — 1

Dr. Alan Winder
MSB Systems, Inc.
110-16 72nd Avenue
Forest Hills, New York 11375 — 1

Dr. T. G. Birdsall
Cooley Electronics Laboratory
University of Michigan
Ann Arbor, Michigan 48105 — 1

Dr. Harry DeFerrari
University of Miami
Rosenstiel School of Marine and
Atmospheric Sciences
Miami, Florida 33149 — 1

Mr. Robert Cunningham
Bendix Electronics Center
15825 Roxford Street
Sylmar, California 91342 — 1

Dr. Stephen Wolff
John Hopkins University
Baltimore, Maryland 21218 — 1

DISTRIBUTION LIST - 5

Dr. M. A. Basin
S. D. P., Inc.
15250 Ventura Boulevard, Suite 518
Sherman Oaks, California 91403 — 1

Commanding Officer
New London Laboratory
Naval Underwater Systems Center
New London, Connecticut 06320
ATTN: Dr. Albert Nuttall — 1

Dr. Walter Duing
University of Miami
Rosenstiel School of Marine and
Atmospheric Sciences
Miami, Florida 33149 — 1

Commanding Officer
New London Laboratory
Naval Underwater Systems Center
New London, Connecticut 06320
ATTN: Dr. H. W. Marsh
Dr. D. M. Viccione — 1

Dr. David Middleton
127 East 91st Street
New York, New York 10028 — (Uncl.) 1

Dr. David Middleton
c/o ONR New York Area Office
207 West 24th Street
New York, New York 10011 — (Class.) 1

Dr. Donald W. Tufts
University of Rhode Island
Kingston, Rhode Island 02881 — 1

Dr. Loren W. Nolte
Department of Electrical Engineering FT-10
University of Washington
Seattle, Washington 98195 — 1

Mr. S. W. Autrey
Hughes Aircraft Company
P. O. Box 3310
Fullerton, California 92634 — 1

Dr. Thomas W. Ellis
Texas Instruments, Inc.
13500 North Central Expressway
Dallas, Texas 75231 — 1

DISTRIBUTION LIST - 6

Mr. Robert Swarts Applied Physics Laboratory University of Washington 1013 Northeast Fortieth Street Seattle, Washington 98195	1
Institute for Acoustical Research Miami Division of the Palisades Geophysical Institute 615 S. W. 2nd Avenue Miami, Florida 33130 ATTN: Mr. M. Kronengold Dr. J. Clark Dr. C. Kimball	2
Mr. Carl Hartdegen Palisades Geophysical Institute Sofar Station FPO New York 09560	1
Mr. Charles Loda Institute for Defense Analyses 400 Army-Navy Drive Arlington, Virginia 22202	1
Mr. Beaumont Buck Polar Research Laboratory 123 Santa Barbara Avenue Santa Barbara, California 93101	1
Dr. M. Weinstein Underwater Systems, Inc. 8121 Georgia Avenue Silver Spring, Maryland 20910	1
Dr. Thomas G. Kincaid General Electric Company P. O. Box 1088 Schenectady, New York 12301	1
Applied Research Laboratories The University of Texas at Austin P. O. Box 4029 Austin, Texas 78712 ATTN: Dr. Lloyd Hampton Dr. Charles Wood Dr. T. D. Plemons	4
Woods Hole Oceanographic Institute Woods Hole, Massachusetts 02543 ATTN: Dr. Paul McElroy Mr. R. Porter Mr. R. Spindel	1

DISTRIBUTION LIST - 7

Dr. John Bouyoucos Hydroacoustics, Inc. 321 Northland Avenue P. O. Box 3818 Rochester, New York 14610	1
Systems Control, Inc. 260 Sheridan Avenue Palo Alto, California 94306 ATTN: Mr. L. Seidman	1
Atlantic Oceanographic and Meteorological Laboratories 15 Rickenbacker Causeway Miami, Florida 33149 ATTN: Dr. John Proni	1
Dr. C. N. K. Mooers University of Miami Rosenstiel School of Marine and Atmospheric Sciences 10 Rickenbacker Causeway Miami, Florida 33149	1

Unclassified

SECURITY CLASSIFICATION OF THIS PAGE (When Data Entered)

REPORT DOCUMENTATION PAGE		READ INSTRUCTIONS BEFORE COMPLETING FORM
1. REPORT NUMBER RPI Math. Rep. No. 121	2. GOVT ACCESSION NO.	3. RECIPIENT'S CATALOG NUMBER
4. TITLE (and Subtitle) CONSISTENT ENVIRONMENTAL ACOUSTICS: APPLICATION TO STOCHASTIC INTERNAL-WAVE MODELS		5. TYPE OF REPORT & PERIOD COVERED Technical Report 6. PERFORMING ORG. REPORT NUMBER
7. AUTHOR(s)		8. CONTRACT OR GRANT NUMBER(s) N 00014-76-C-0288
9. PERFORMING ORGANIZATION NAME AND ADDRESS Rensselaer Polytechnic Institute Troy, New York 12181		10. PROGRAM ELEMENT, PROJECT, TASK AREA & WORK UNIT NUMBERS NR 386-606
11. CONTROLLING OFFICE NAME AND ADDRESS Office of Naval Research, Code 222 Department of the Navy Arlington, Virginia 22217		12. REPORT DATE 1 December 1978 13. NUMBER OF PAGES 68
14. MONITORING AGENCY NAME & ADDRESS(if different from Controlling Office)		15. SECURITY CLASS. (of this report) 15a. DECLASSIFICATION/DOWNGRADING SCHEDULE

16. DISTRIBUTION STATEMENT (of this Report)

This document has been approved for public release and sale; its distribution is unlimited.

17. DISTRIBUTION STATEMENT (of the abstract entered in Block 20, if different from Report)

18. SUPPLEMENTARY NOTES

19. KEY WORDS (Continue on reverse side if necessary and identify by block number)

Environmental Acoustics
Internal Waves
Acoustical Statistics

20. ABSTRACT (Continue on reverse side if necessary and identify by block number)

A consistent environmental-acoustic model for a deep moving ocean is formulated. The acoustic model for regularly-perturbed SOFAR rays is approximately solved using a type of WKB(J) expansion. Interfacing conditions between the hydrodynamics and acoustics are developed which lead to constraints on acoustic frequency and transmission range. As an application, → next page (over please)

DD FORM 1 JAN 73 1473 EDITION OF 1 NOV 65 IS OBSOLETE
S/N 0102-LF-014-6601

Unclassified

SECURITY CLASSIFICATION OF THIS PAGE (When Data Entered)

transmissions are considered through stochastic internal-wave fields, which have been modeled in a previously-published paper by the authors. Formulas for ray phase variances are derived. These formulas are asymptotically evaluated for rays with relatively significant depth variation, using the stationary phase method. New results are obtained for the dependence of the variances on internal-wave primitives, such as energy spectra. Expected multipath intensity is calculated for transmission through an ocean with static state modeled by a bilinear sound-speed profile. The effects of the internal-wave field and of varying internal-wave parameters on the expected intensity are shown to be significant.